KfK 5426
RUB E-75
Dezember 1994

The Release Code Package REVOLS/RENONS for Fission Product Release from a Liquid Sodium Pool into an Inert Gas Atmosphere

J. Starflinger, M. K. Koch, U. Brockmeier,
W. Schütz, W. Scholtyssek, H. Unger
Institut für Neutronenphysik und Reaktortechnik
Projekt Nukleare Sicherheitsforschung

Kernforschungszentrum Karlsruhe

KERNFORSCHUNGSZENTRUM KARLSRUHE

Institut für Neutronenphysik und Reaktortechnik

Projekt Nukleare Sicherheitsforschung

KfK 5426

RUB E-75

The Release Code Package REVOLS/RENONS for Fission Product Release from a Liquid Sodium Pool into an Inert Gas Atmosphere

J. Starflinger*, M.K. Koch*, U. Brockmeier*, W. Schütz,

W. Scholtyssek, H. Unger*

* Department for Nuclear and New Energy Systems,
Ruhr University of Bochum, 44780 Bochum, Germany

This work was supported by the European Atomic Energy Community under Contract No: ETNU-CT92-0077

Kernforschungszentrum Karlsruhe GmbH, Karlsruhe

Als Manuskript gedruckt

Kernforschungszentrum Karlsruhe GmbH
Postfach 3640, 76021 Karlsruhe

ISSN 0303-4003

Abstract

For aerosol source term considerations in the field of nuclear safety, the investigation of the release of volatile and non–volatile species from liquid surfaces into a gas atmosphere is important. In case of a hypothetical liquid metal fast breeder reactor accident with tank failure, primary coolant sodium with suspended or solved fuel particles and fission products may be released into the containment. The computer code package REVOLS/RENONS, based on a theoretical mechanistic model with a modular structure, has been developed for the prediction of sodium release as well as volatile and non–volatile radionuclide release from a liquid pool surface into the inert gas atmosphere of the inner containment. Hereby the release of sodium and volatile fission products, like cesium and sodium iodide, is calculated using a theoretical model in a mass transfer coefficient formulation. This model has been transposed into the code version REVOLS.MOD1.1, which is discussed here. It enables parameter analysis under highly variable user-defined boundary conditions. Whereas the evaporative release of the volatile components is governed by diffusive and convective transport processes, the release of the non–volatile ones may be governed by mechanical processes which lead to droplet entrainment from the wavy pool surface under conditions of natural or forced convection into the atmosphere. The mechanistic model calculates the liquid entrainment rate of the non–volatile species, like the fission product strontium oxide and the fuel (uranium dioxide) from a liquid pool surface into a parallel gas flow. The mechanistic model has been transposed into the computer code package REVOLS/RENONS, which is discussed here. Hereby the module REVOLS (RElease of VOLatile Species) calculates the evaporative release of the volatile species, while the module RENONS (RElease of NON–Volatile Species) computes the entrainment release of the non–volatile radionuclides. Hence, e.g. the influence of the pool surface– and gas temperatures, the pool inventory and the geometry as well as the decisive influence of the thermal hydraulic conditions on the release rate can be investigated.

Das Programmsystem REVOLS/RENONS für Spaltproduktfreisetzung aus einem Pool mit Flüssignatrium in eine Inertgasatmosphäre

Kurzfassung

Im Rahmen der Reaktorsicherheitsanalyse ist die Verbesserung der Modelle zur Berechnung von Aerosolquellltermen für die Untersuchung des Freisetzungsverhaltens flüchtiger und schwer flüchtiger Stoffe von Flüssigkeitsoberflächen in eine Inertgasatmosphäre von Bedeutung. Unter der Voraussetzung eines hypothetischen Unfalls mit Tankversagen bildet sich im inneren Containment eines Schnellen Natriumgekühlten Reaktors ein Natriumpool aus, der mit gelösten oder dispergierten Radionukliden kontaminiert sein kann. Zur Beschreibung der Freisetzung des Primärkühlmittels Natrium sowie flüchtiger (Cäsium, Rubidium, Natriumjodid) und schwer flüchtiger Radionuklide (Strontiumoxid, Urandioxid) von einer Pooloberfläche in eine Inertgasatmosphäre wird ein mechanistisches Modell mit einer modularen Struktur entwickelt. Dieser mechanistische Modellansatz ist in die hier diskutierte Programmversion REVOLS.MOD1.1 umgesetzt worden, welche Parametervariationsrechnungen bei möglichst variablen, durch den Nutzer wählbaren Randbedingungen ermöglicht. Während die Freisetzung der flüchtigen Stoffe somit durch diffusive und konvektive Transportprozesse bestimmt wird, wird die der schwer flüchtigen maßgeblich durch mechanische Prozesse verursacht, durch die bei freier oder erzwungener Konvektion in der Gasphase Flüssigkeitstropfen mit darin dispergierten Radionuklidpartikeln von der welligen Oberfläche in den Gasstrom mitgerissen werden. Das mechanistische Modell ist in das hier diskutierte Programmpaket REVOLS/RENONS umgesetzt. Hierbei bestimmt der Modul REVOLS (RElease of VOLatile Species) die Freisetzung der flüchtigen, der Modul RENONS (RElease of NON–Volatile Species) die der schwer flüchtigen Stoffe. Somit steht ein Instrument zur Verfügung, mit dem die Einflüsse der Pooloberflächen– und Gasbulktemperatur, des Poolinventars und der Geometrie sowie der maßgebliche Einfluß der thermohydraulischen Bedingungen in der Gasatmosphäre auf das Natrium– und Radionuklidfreisetzungsverhalten untersucht werden können.

Contents

Nomenclature

Latin Symbols

A, m, n	$[-]$	constants in heat/mass transfer correlation (Eqs. 3.9 and 3.10)
A_2, A_4, B_2, B_4	$[-]$	constants (Eq. 4.39)
b	$[m]$	pool width
c	$[-]$	mass fraction
c_1	$[-]$	correction coefficient for one-directional diffusion treatment
c_{cond}	$[-]$	correction coefficient for condensation effects
c_ρ	$[-]$	correction coefficient for gas phase mass concentration
c_p	$[J/kgK]$	specific heat capacity
d	$[m]$	droplet diameter
D	$[m^2/s]$	binary diffusion coefficient
g	$[m/s^2]$	gravitational acceleration
h	$[m]$	effective wave height
Δh_F	$[kJ/kg]$	heat of formation of molecules (Eqs. 4.34 and 4.35)
Δh_V	$[kJ/kg]$	latent heat of vaporization
K	$[-]$	von Karman constant
K_τ	$[-]$	constant
k_2	$[1/bar]$	equilibrium constant (Eq. 4.37)
k_4	$[1/bar^3]$	equilibrium constant (Eq. 4.38)
L	$[m]$	characteristic length
$\tilde{M}_A$	$[g/mole]$	molecular weight of species A
$\dot{M}$	$[kg/s]$	mass flow
m	$[kg]$	mass

$\dot{m}$	$[kg/m^2s]$	mass flux
$\dot{n}_d$	$[1/m^2s]$	droplet flux density
$\dot{n}_{d*}$	$[1/m^2s]$	normalized droplet flux density
p	$[Pa]$	system pressure
p_A	$[Pa]$	partial pressure of species A
p_v	$[Pa]$	equilibrium vapor pressure
$\acute{p}$	$[Pa/K]$	derivative $\partial p/\partial T$ with $p(T)$
$p^\star$	$[-]$	dimensionless pressure
R	$[J/moleK]$	universal gas constant
RF	$[-]$	retention factor
s	$[m]$	thickness of the phase interface
T	$[K]$	temperature
$\bar{T}$	$[K]$	mean temperature
u	$[m/s]$	velocity in the boundary layer
U_∞	$[m/s]$	velocity outside the boundary layer
u_*	$[m/s]$	friction velocity
$\bar{v}$	$[m/s]$	mean velocity
X	$[-]$	molar concentration
x	$[m]$	horizontal direction
z	$[m]$	vertical direction
z_d	$[m]$	droplet layer thickness

Greek Symbols

α	$[W/m^2K]$	heat transfer coefficient
β	$[m/s]$	mass transfer coefficient
γ	$[-]$	activity coefficient
δ	$[m]$	boundary layer thickness
ρ	$[kg/m^3]$	density

ρ_A	$[kg/m^3]$	partial density of the species A
$\Delta\rho$	$[kg/m^3]$	density difference
η	$[kg/ms]$	dynamic viscosity
λ	$[W/mK]$	thermal conductivity
μ^E	$[J/mole]$	excess Gibbs energy
ν	$[m^2/s]$	kinematic viscosity
τ	$[Pa]$	shear stress
ω	$[-]$	exponent in Eq. 3.16

Subscripts

A	species
Ar	argon
b	boiling
Cs	cesium
$cond$	condensation
E	entrainment
eqm	equimolar
FP	fission product
F	formation
g	gas phase
L	solvent (here: Na)
l	liquid phase
max	maximum value
min	minimum value
Na	sodium
NaI	sodium iodide
NFP	non-volatile fission product and fuel particles
N_2	nitrogen

Ph	phase interface
$Pool$	pool
Rb	rubidium
S	surface
sat	saturation
VFP	volatile fission product
v	equilibrium vapor state
∞	state outside boundary layers
$*$	dimensionless
0	initial state
1	one-directional

Dimensionless Symbols

$Gr = \frac{\rho^2 \cdot g \cdot L_{ch}^3}{\eta^2} \cdot \left(\frac{T_{Ph}}{T_\infty} \cdot \frac{\tilde{M}_\infty}{\tilde{M}_{Ph}} - 1 \right)$	Grashof number
$Le = Sc/Pr$	Lewis number
$Nu = \frac{\alpha \cdot L_{ch}}{\lambda}$	Nusselt number
$Pr = \frac{\eta \cdot c_p}{\lambda}$	Prandtl number
$Ra = Gr \cdot Pr$	Rayleigh number
$Re = \frac{\bar{v} \cdot L_{ch}}{\nu}$	Reynolds number

$Re_h = \frac{u_* \cdot h}{\nu_g}$	Wave Reynolds number
$Re_{z_d} = \frac{u_* \cdot z_d}{\nu_g}$	Droplet-Layer Reynolds number
$Sc = \frac{\eta}{\rho \cdot D}$	Schmidt number
$Sh = \frac{\beta \cdot L_{ch}}{D}$	Sherwood number

1 Introduction

For aerosol source term considerations in the field of nuclear safety, it is important to investigate the release of volatile and non–volatile species from liquid surfaces into a gas atmosphere. In case of a hypothetical liquid metal fast breeder reactor (LMFBR) accident with tank failure, primary coolant sodium with suspended or solved fuel particles and fission products may be released into the containment. The code package REVOLS/RENONS calculates, based on theoretical mechanistic models, the release of these volatile and non–volatile species from a liquid pool into the inert gas atmosphere of the inner containment. Hereby, the module REVOLS calculates the RElease of VOLatile Species [1–3]. This module is based on a theoretical mechanistic model in a mass transfer coefficient formulation, which assumes the mass flux of the volatiles to be controlled by a driving force, here the partial density difference between the gas side of the liquid surface and the atmosphere, and the mass transfer coefficient, denoting the reciprocal resistance of the species against mass transfer. Whereas the evaporative release of the volatile species is governed by diffusive and convective transport processes, the release of the non–volatile ones may be governed by mechanic processes which lead to droplet entrainment from the wavy pool surface under conditions of natural or forced convection in the atmosphere. The module RENONS (RElease of NON–volatile Species) calculates the liquid entrainment rate of non–volatile species from liquid pool surfaces into a parallel gas flow [4, 5]. The mechanistic model for the entrainment rate calculation is based on a droplet flux formulation with the droplet flux being a function of the friction velocity at the wavy surface, the wave height and the fluid properties of liquid and gas. In the code package, the release of the solvent — here sodium — is described in terms of a mass flux. The release of the suspended or solved species, like fission products and fuel, is described in terms of a retention factor expression [6–8].

2 Technical Background

The background of the mechanistic model and computer code development is given by the LMFBR safety analysis and the development of the CONTAIN code release modules [9]. Assuming a hypothetical accident with reactor vessel failure, a sodium pool is formed in the inner containment which may be contaminated with fission products and fuel. This long term aerosol source S_2 is governed by the release of primary coolant sodium, solute volatile and dispersed non–volatile fission products and fuel from the liquid pool into the inert gas atmosphere of the inner containment. Figure 1 shows a schematic cross section of a part of a LMFBR containment (SNR-300 conditions, [10]) in a state following a tank failure.

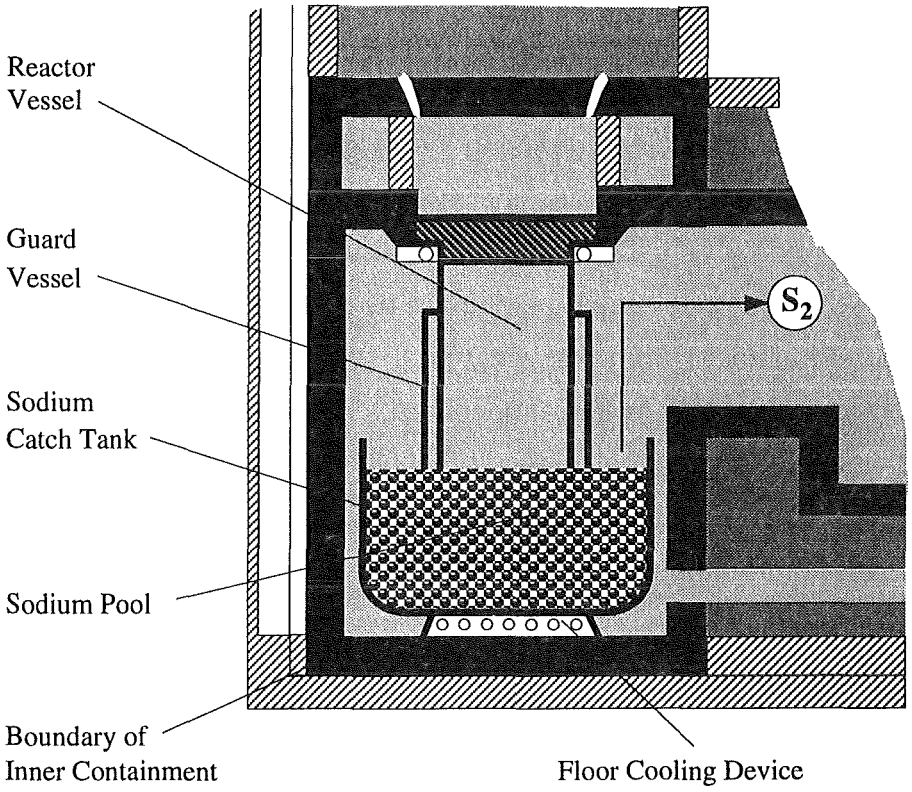

Fig. 1: Schematic cross section of a part of a liquid metal fast breeder reactor containment with the long term aerosol source S_2, assuming a hypothetical accident with tank failure [10].

For the improvement of radioactive source term calculations, the code package REVOLS/RENONS, as the first one of its kind, is based on a mechanistic model (Chapter 3), developed to be coupled to severe accident containment analysis codes.

3 Mechanistic Model

For a systematical investigation of fission product (FP) release behavior, the arrangement of the radionuclides treated is chosen according to their volatility, which has been identified to be a decisive classification to describe the different species' release mechanisms. Hence, in the first instance the radionuclides treated fall into three release categories, namely inert (I), volatile (II) and low– or non–volatile (III). These individual categories are again subdivided into so-called release groups with their organization assigned according to the chemical affinity of the species considered.

Category I contains only one group (Group 1) with the noble gases (e.g. xenon, krypton). Due to their high volatility, the noble gases are almost immediately virtually totally released, so that no further investigation is required here.

The volatile species of Category II are summarized in Group 2 to 4. Group 2 stands for halogens (e.g. iodine, bromine), Group 3 contains the alkali metals (e.g. sodium, rubidium or cesium), i.e. the coolant sodium as well as volatile fission products, and Group 4 with the chalcogens (e.g. tellurium) and elements of the nitrogen group (e.g. antimony).

The Category III of low– or non–volatile radionuclides is represented by Group 5 with the alkaline–earth metals (strontium, barium) and by Group 6 consisting of transition metals (cobalt, molybdenum and ruthenium) as well as Group 7 containing the lanthanides, and the actinide elements uranium, plutonium and americium. Hereby, the volatility of the respective species continuously decreases from the first to the last group [11].

Besides the coolant sodium, which is of importance just because of the considerably high amount of mass released, characteristic elements of the Categories II and III which are important for the severe accident analysis are taken into consideration for the development of the release model described in Chapter 3.1 and 3.2.

Main emphasis has been placed on the volatile and simultaneously radioactive short–termed effective fission products of the Groups 2 and 3 (Category II), because besides of their relatively high volatility they often show a relatively long half–life of several years and a substantial biological effectivity.

Considering the volatile fission products, another subdivision into non–reacting (so-called metallic) and molecule forming species, the latter with high electronegativity, is appropriate. In the pool, the metallic group, consisting of the highly volatile fission products cesium and rubidium (Group 2), is assumed to exist simply solved on the base of a thermodynamic behavior similar to the solvent sodium. Under reactor accident conditions, the electronegative fission products iodine and bromine of Group 3 react with sodium to form the halides sodium iodide and sodium bromide. These molecules are less volatile compared to the halogens.

In a highly burned–up fuel, the bromine mass is about eighty times smaller than the iodine mass [12]. Since in addition, the half–life of the bromine isotope is rather short (some minutes only), iodine and sodium iodide are important for the release only. Consequently, the bromine can be neglected.

From Category III, the fission product strontium reacts under reactor accident conditions to strontium oxide [7, 8], while uranium appears as uranium dioxide. In case of an accidental release, the radioactive strontium isotope ^{90}Sr with a half–life of about 28 years is especially dangerous because it accumulates mainly in the bones [13] after ingestion. The LMFBR fuel normally is a mixture of uranium– and plutonium oxides. Both compositions are similar with respect to the decisive physical and chemical properties, therefore representatively only the uranium dioxide release will be discussed further.

In order of their appearance in the categories listed above, the release mechanisms of volatile species are discussed in detail in the following Chapter 3.1, as well as in Chapter 3.2 for the non–volatile ones.

3.1 Volatile Fission Product Release

Concerning the volatile fission product (VFP) release, the liquid pool and the inert gas atmosphere of the inner containment are assumed to be acting as a two–phase system with the mass transfer governed by diffusive and convective transport processes. Such a system is sketched in Fig. 2, in which the phase interface is depicted enlarged to point out the coupled states of the partial density ρ_A of the species A in both phases (index: $g \mathrel{\widehat{=}}$ gas phase, $l \mathrel{\widehat{=}}$ liquid phase) on both sides of the phase interface (index: Ph).

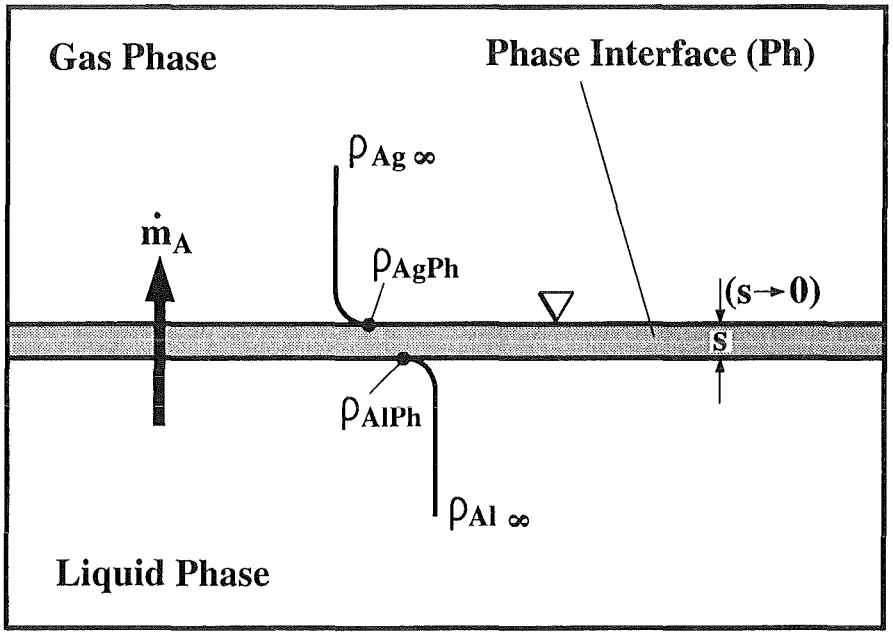

Fig. 2: Sketch of a two phase system — gas atmosphere and liquid pool — separated by the phase interface, with the release mass flux $\dot{m}_A$ of the respective species A in the pool, and the partial density profile of the species A with $\rho_{Al\infty}$ in the liquid phase outside of and ρ_{AlPh} at the liquid side of the phase interface, as well as ρ_{AgPh} at the gas side, and $\rho_{Ag\infty}$ in the gas phase outside the concentration boundary layer.

Here, Fig. 2 shows a typical course of an exemplary partial density profile, with a decrease of the partial density ρ_A of the species A from the liquid phase bulk (index: $l\infty$) to the liquid side of the phase interface (index: lPh), a leap of the

partial density over the phase interface caused by phase equilibrium conditions and a further decrease of the partial density from the gas side of the phase interface (index: gPh) into the bulk of the gas phase (index: $g\infty$).

Hence, the theoretical mass transfer model is based on the so-called mass transfer coefficient formulation, which assumes the mass flux $\dot{m}_A$ of a volatile species A to be controlled by a driving force, i.e. the partial density difference $\Delta\rho_{Ag}$ between liquid surface and gas bulk (index: g), and the mass transfer coefficient β_{Ag} denoting the reciprocal resistance against mass transfer. Hence, the release mass flux $\dot{m}_A$ of any volatile species A ($A \mathrel{\hat{=}} Na$ as well as Cs, Rb, NaI) can be expressed by:

$$\dot{m}_A = \beta_{Ag} \cdot \Delta\rho_{Ag} \ , \tag{3.1}$$

with the mass transfer coefficient β_{Ag} of the species A in the gas phase (g) given as:

$$\beta_{Ag} = Sh_{Ag} \cdot \frac{D_{Ag}}{L} \quad . \tag{3.2}$$

In Eq. 3.2 the mass transfer coefficient β_{Ag} is basically a function of the mass transfer conditions considered indicated by the Sherwood number Sh_{Ag}, and the binary diffusion coefficient D_{Ag} of the species A in the gas phase as well as the characteristic length L of the respective geometry, e.g. the diameter of the liquid pool considered (see Fig. 1).

The partial density difference $\Delta\rho_{Ag}$ (Eq. 3.1) of the species A in the gas phase between the phase interface (index: Ph) of the liquid surface and the bulk of the gas phase (index: $g\infty$) is given as depicted in Fig. 2 by:

$$\Delta\rho_{Ag} = \rho_{AgPh} - \rho_{Ag\infty} \quad . \tag{3.3}$$

Here, $\rho_{Ag\infty}$ is determined from mass balance considerations in the bulk atmosphere, i.e.

$$\rho_{Ag\infty} = f\left(\dot{M}_A, \rho_{Ag\infty}|_0\right) \ , \tag{3.4}$$

with the mass flow $\dot{M}_A$ of the evaporating species into the atmosphere and its initial partial density $\rho_{Ag\infty}|_0$. Considering the solved fission products, because of the small amount of volatile fission products (VFP) denoting the pool inventory, $\rho_{VFP\,g\infty} = 0$ can be assumed. In case of sodium evaporation, the liquid solvent of the pool, the raising amount of sodium in the gas phase can be expressed by a special correction coefficient (see Chapter 3.1.2).

With the understanding that the VFP and the solvent sodium are a real but highly diluted solution, and assuming the released volatile species A acting as a perfect gas under gas condition, the partial density ρ_{AgPh} of the species A at the gas side of the phase interface is given by:

$$\rho_{AgPh} = \frac{p_{vA}(T_{Ph})}{R/M_A \cdot T_{Ph}} \cdot \gamma_A \cdot c_A \quad , \tag{3.5}$$

with c_A denoting the mass concentration of the species A (e.g. VFP) in the liquid, and the quantity γ_A denoting the so called activity coefficient with [14]:

$$\gamma_A = \exp\left(\frac{\mu_A^E}{RT}\right) \quad . \tag{3.6}$$

The excess Gibbs energy ${}_l\mu_A^E$ is given in [12, 15–18] for different fission products A as a function of the temperature T assuming constant system pressure and small fission product concentrations in the solvent.

In case of sodium evaporation, $\gamma_A = c_A = 1$ is a satisfactory approximation due to the small amount of fission products in the liquid sodium pool.

The equilibrium vapor pressure p_{vA} as a function of the temperature in Eq. 3.5 may be taken from [19–25] (see Chapter 4.2).

As in common use, all liquid phase properties, involved in the above and following equations are evaluated at the phase interface temperature T_{Ph}. However, the gas phase properties are calculated at the so-called film temperature of the gas side boundary layer defined as:

$$\bar{T} = \frac{T_{Ph} + T_{g\infty}}{2} \quad , \tag{3.7}$$

with the phase interface temperature T_{Ph}, and the temperature $T_{g\infty}$ of the gas atmosphere outside the boundary layer.

According to Eq. 3.2 it is obvious that the mass transfer condition considered has valuable influence on the release of sodium and volatile fission products. These evaporation conditions are determined by the dimensionless Sherwood number Sh_{Ag} and discussed in detail in the next Chapter 3.1.1.

3.1.1 Heat and Mass Transfer Correlations

The Sherwood number Sh_{Ag} in Eq. 3.2 used to calculate the mass transfer coefficient β_{Ag} can be derived from the equimolar counterdiffusion Sherwood number $Sh_{Ag\ eqm}$ and two later (see Chapter 3.1.2) discussed correction coefficients c_{1A} denoting different defects in the analogy of heat and mass transfer and $c_{cond\ A}$ for consideration of re-condensation (i.e. fog formation) within the thermal boundary layer on the gas side of the phase interface:

$$Sh_{Ag} = Sh_{Ag\,eqm} \cdot c_{1A} \cdot c_{condA} \quad . \tag{3.8}$$

Assuming the analogy between heat and mass transfer for the case of equimolar counterdiffusion at the phase interface, the convective mass transfer Sherwood number $Sh_{Ag\ eqm}$ may be derived from correlations concerning the corresponding heat transfer Nusselt number Nu_g (see Eq. 3.9) mostly already implemented in the corresponding safety codes, e.g. CONTAIN [26, 27], for heat flux calculations. For example in case of free convection, dimensionless correlations for the heat transfer data are usually given as a function of the Grashof number Gr_g for temperature driven free convection and the Prandtl number Pr_g:

$$Nu_g = A \cdot Gr_g^m \cdot Pr_g^n \quad . \tag{3.9}$$

In case of forced convection in the gas phase, in Eq. 3.9 the Grashof number Gr_g has to be replaced by the Reynolds number Re_g. Consequently, the mass

transfer controlled by temperature driven free convection can be correlated by the same function, if the Prandtl number Pr_g is replaced by the Schmidt number Sc_{Ag} of the species A ($A \mathrel{\widehat{=}} Na$ or VFP).

Hence, the Sherwood number $Sh_{Ag\ eqm}$ is given as a function of the dimensionless Grashof Gr_g and Schmidt number Sc_{Ag} using the general expression:

$$Sh_{Ag\,eqm} = A \cdot {Gr_g}^m \cdot Sc_{Ag}^n \quad , \tag{3.10}$$

with the coefficients A, m and n corresponding to the respective heat transfer situations. For examples, three of them are sketched below:

1. **Hot pool surface/ cold atmosphere:**
   Based on detailed investigations of heat transfer conditions at horizontal flat plates of different size and geometry [28], the coefficients are worked out as an accommodation of experimental mass transfer data derived from the NALA I [7] and NALA II experiments [8] of the Karlsruhe Research Center to consider the liquid phase interface of the pool:

$$\begin{aligned} A &= 0.76, \\ m = n &= 0.305, \end{aligned} \tag{3.11}$$

   being independent from a laminar or turbulent flow regime. Resulting from comparative assessment of several heat transfer correlations [28, 29], the corresponding validity range is $2 \cdot 10^5 \leq Ra_g \leq 10^{13}$, with the Rayleigh number Ra_g as the product of the Grashof number Gr_g and the Prandtl number Pr_g.

2. **Cold pool surface/ hot atmosphere:**
   Corresponding to the governing heat transfer correlation implemented in the CONTAIN code [26, 27] for this heat transfer process, the following coefficients are used:

$$\begin{aligned} A &= 0.27, \\ m = n &= 0.25. \end{aligned} \tag{3.12}$$

3. **Convection caused by external heat sources/ sinks:**
   In this case the current code version REVOLS.MOD1.1 calculates an equimolar Sherwood number using the expression:

$$Sh_{Ag\,eqm} = Nu_g \cdot \left(\frac{Sc_{Ag}}{Pr_g}\right)^{1/3} . \tag{3.13}$$

   The Nusselt number Nu_g for the calculation is submitted by the corresponding safety code, e.g. CONTAIN.

In Eq. 3.9 and 3.10 the Grashof number is defined as [30]:

$$Gr_g = \frac{L^3 \cdot g \cdot \rho_g^2}{\eta_g^2}\left(\frac{\tilde{M}_{g\infty}}{\tilde{M}_{Ph}} \cdot \frac{T_{Ph}}{T_{g\infty}} - 1\right) \quad , \tag{3.14}$$

with the characteristic length L (see Eq. 3.2), the gravitational acceleration g, the boundary layer gas density ρ_g, dynamic viscosity η_g, the molecular weights of the gas phase $\tilde{M}_{g\infty}$ and $\tilde{M}_{Ph}$ and the gas temperatures $T_{g\infty}$ and T_{Ph} outside the boundary layer (index: $g\infty$) and at the phase interface (index: Ph), respectively.

The Schmidt number Sc_{Ag} is defined as

$$Sc_{Ag} = \frac{\eta_g}{\rho_g \cdot D_{Ag}} \quad , \tag{3.15}$$

with η_g and ρ_g correlated in Chapter 4.1 and D_{Ag} as in Eq. 4.17.

The dimensionless groups — Grashof Gr_g or Reynolds number Re_g for free and forced convection respectively, Prandtl number Pr_g for heat transfer and Schmidt number Sc_{Ag} for mass transfer — allow for an upscaling of laboratory data to realistic scenarios, as long as true similarity between the laboratory scale and the technical scale situation can be assumed. The characteristic length L of the geometry entering the dimensionless groups governs the upscaling process. Depending on the problem, the characteristic length L might be the pool diameter, the height of a vertical wall or the pathway of a flow around an obstacle. If the similarity is not ensured, the corresponding

correlations might fail when treating upscaled geometries. In any case, at least consistency is maintained as long as analogous mass transfer correlations are derived from heat transfer correlations already operating in the safety codes under consideration.

3.1.2 Correction Factors

The mechanistic release model is based on the assumptions that the evaporating sodium is transported into the atmosphere in perpendicular direction to the liquid surface, and that the inert gas molecules (atoms in case of argon) are not able to push through the liquid surface [2]. The result is a one-directional diffusion mass flow of evaporating sodium. To obtain the conditions described above, an additional sodium flow is required to repulse the moving inert gas atoms back into the gas phase. This additional (convective) flow (the so-called Stefan flow) is a characteristic difference between one-directional and equimolar counterdiffusion.

One-Directional Diffusion

The correction coefficient c_{1A} ($A \mathrel{\widehat{=}} Na, VFP$) characterizes the one-directional diffusion for both low and high evaporation mass fluxes [31], similarly representing the defect of ideal analogy between (convective) heat and (one-directional diffusion) mass transfer, instead of equimolar counterdiffusion treatment. It is governed by the expression:

$$c_{1A} = \left[p^{\star} \cdot \ln \frac{p^{\star}}{p^{\star} - 1} \right]^{\omega} \cdot \left(\frac{p}{p - p_{AgPh}} \right) \quad , \tag{3.16}$$

with the dimensionless pressure

$$p^{\star} = \frac{p - p_{AgPh}}{p_{Ag\infty} - p_{AgPh}} \quad . \tag{3.17}$$

In Eqs. 3.16 and 3.17, the quantity p is the system pressure and p_{AgPh} as well as $p_{Ag\infty}$ are the partial pressures of the species A in the gas phase at the interface (index: Ph) and outside the boundary layer (index: $g\infty$) respectively. The correction coefficient c_{1A} expresses the ratio of the one-directional (index: 1) and equimolar (index: eqm) Sherwood number:

$$c_{1A} = \frac{Sh_{Ag\ 1}}{Sh_{Ag\ eqm}} \quad . \tag{3.18}$$

For low partial pressures, dependent on the dimensionless pressure function $p^* \cdot ln[p^*/(p^* - 1)]$ the one-directional Sherwood number $Sh_{Ag\ 1}$ has been analyzed for several experiments, reflecting the equimolar counterdiffusion limit:

$$\lim_{\text{partial pressure}\to 0} Sh_{Ag\ 1} = Sh_{Ag\ eqm} \ .$$

The evaluation of experimental data in [31] led to an exponent $\omega = 1.22$, resulting in appropriate values even for high sodium evaporation rates. As a satisfactory first guess c_{1A} from Eq. 3.16 is also valid for turbulent flow and other than plate shapes [31].

Condensation in the Boundary Layer above the Pool

The second correction coefficient $c_{cond\ A}$ in Eq. 3.8 treats the enhancement of evaporation rates of liquids in cooler environments, caused by condensation within the thermal boundary layer.

In case of evaporation from a hot pool surface into a cooler atmosphere, the evaporating steam starts from the surface with a partial pressure corresponding to the saturation pressure at pool surface temperature. In the course of its way through the temperature boundary layer, the steam passes cooler regions leading to a supersaturation state of the steam. Depending on the model (equilibrium or non–equilibrium condensation), the steam state "falls back" to the saturation state corresponding to the local temperature at each position in the thermal boundary layer, either instantaneous (equilibrium model) or allowing

for a certain supersaturation to exist (supersaturation model). In both cases, the residual steam above the partial pressure allowed to exist in the boundary layer is assumed to condensate. This results in a corresponding decrease of the steam volume in the mass transfer boundary layer and in turn in an increase of the partial pressure gradient at the pool surface. This increase again leads to an increase in the mass transfer rate. The used correlation:

$$c_{condA} = \sqrt{c_{cond\,A\,max} \cdot c_{cond\,A\,min}} \tag{3.19}$$

is based on a correlation for the equilibrium case reflecting the maximum possible mass transfer increase $c_{cond\ A\ max}$. The geometric mean has been taken as a first approximation to account for non–equilibrium caused reductions according to experimental data reported in [32, 33].

In Eq. 3.19, the quantity $c_{cond\ A\ min}$ denotes the minimum case, in which no condensation occurs within the thermal boundary layer. It is simply given by $c_{cond\ A\ min} = 1$, i.e. already the minimum value of $c_{cond\ A}$. The maximum case, denoted by $c_{cond\ A\ max}$, is governed by the following expression [34]:

$$c_{cond\,A\,max} = \frac{\acute{p}_{vA}(T_{Ph}) \cdot \left(\Delta T \cdot Le_{Ag}^{-n} + (\Delta h_{VA} \cdot \Delta p_A)/\left(Le_{Ag} \cdot c_{p\,g} \cdot p\right)\right)}{\Delta p_A \cdot \left(1 + (\acute{p}_{vA}(T_{Ph}) \cdot \Delta h_{VA})/\left(Le_{Ag} \cdot c_{p\,g} \cdot p\right)\right)} \quad . \tag{3.20}$$

In Eq. 3.20, the expression $\acute{p}_{vA}$ denotes the first derivative of the vapor pressure p_{vA} to the temperature T at the location of the phase interface (Ph), i.e. $\acute{p}_{vA} = \partial p_{vA}/\partial T|_{Ph}$. Other quantities in Eq. 3.20 are the temperature and pressure differences in the gas phase, $\Delta T = T_{Ph} - T_{g\infty}$ and $\Delta p_A = p_{AgPh} - p_{Ag\infty}$ respectively, the specific heat capacity $c_{p\,g}$ of the gas phase and the latent heat of vaporization Δh_{VA} of the evaporating species A. In Eq. 3.20 the dimensionless Lewis number Le_{Ag} is defined as:

$$Le_{Ag} = \frac{Sc_{Ag}}{Pr_g} = \frac{\lambda_g}{\rho_g \cdot D_{Ag} \cdot c_{p\,g}} \quad , \tag{3.21}$$

with the thermal conductivity of the gas phase λ_g and all other symbols in Eq. 3.21 and 3.20 according to the definitions met before. More details regarding the model for $c_{cond\ A\ max}$ can be found in [33–36].

High Atmospheric Sodium Partial Pressures

The code version REVOLS.MOD1.1 considers a non–zero sodium partial pressure in the gas phase using the following correction factor c_ρ:

$$\begin{aligned} \dot{m}_{Na} &= c_\rho \quad \cdot \quad \dot{m}_{Na}\Big|_{\rho_{Nag\infty}\to 0} \\ &= \left(1 - \frac{\rho_{Nag\infty}}{\rho_{Ph}}\right) \cdot \dot{m}_{Na}\Big|_{\rho_{Nag\infty}\to 0} \end{aligned} \tag{3.22}$$

with $\dot{m}_{Na}|_{\rho_{Nag}\to 0}$ reflecting the MOD1-model evaporation rate for $\rho_{Nag\infty} = 0$, and $\dot{m}_{Na}$ reflecting the MOD1.1 evaporation rate for any sodium partial density in the atmosphere $\rho_{Nag\infty}$. The values $\rho_{Nag\infty}$ and ρ_{Phg} denote the partial densities of sodium in the atmosphere and at the phase interface (pool surface), respectively.

Retention Factor

The release of the solvent (here sodium) is described in terms of a mass flux $\dot{m}_L$ ($L \mathrel{\hat{=}} Na$), whereas the release of the solutes (e.g. volatile fission products (VFP)) is considered by introducing a geometry- and state dependent retention factor formulation [2, 7, 8]. The retention factor RF_{VFP} of the volatile species is given by an expression:

$$RF_{VFP} = \frac{\left(\frac{m_{VFP}}{m_L}\right)_{Pool}}{\frac{\dot{m}_{VFP}}{\dot{m}_L}} \quad , \tag{3.23}$$

where m_{APool} (here $A \mathrel{\hat{=}} VFP, L$) denotes the mass inventory of the respective species A in the pool and $\dot{m}_A$ the corresponding evaporative release mass

fluxes of the solute volatile fission product (VFP) and the solvent liquid (L). Based on this mechanistic model, the computer code module REVOLS calculates the release mass fluxes and the retention factors of the volatile species.

Because the solvents and the solutes are underlying identical thermal–hydraulic conditions, the thermal–hydraulics governed by the type of convection, the surface geometry and the system states "divide out", so that the retention factor can be expressed as a function of the fluid properties and system states:

$$RF = \frac{\left(\frac{m_{VFP}}{m_L}\right)_{Pool}}{\left(\frac{D_{VFPg}}{D_{Lg}}\right)^{1-n} \cdot \frac{(c_1 \cdot c_{cond})_{VFP}}{(c_1 \cdot c_{cond})_L} \cdot \frac{\tilde{M}_{VFP}}{\tilde{M}_L} \cdot x_{VFPlPh} \cdot \gamma_{VFP} \cdot \frac{p_{vVFP}}{p_{vL}}} . \tag{3.24}$$

The use of the retention factor formulation for the volatile fission product release has the advantage that as a satisfactorily good approximation the retention factor RF is independent of the concentration conditions in the pool. However, the validity of Eq. 3.24 is restricted to small relative concentrations c of the solute (VFP) in the solvent (Na). This yields to a more simplified expression of the retention factor:

$$RF = \frac{1}{\left(\frac{D_{VFPg}}{D_{Lg}}\right)^{1-n} \cdot \frac{(c_1 \cdot c_{cond})_{VFP}}{(c_1 \cdot c_{cond})_L} \cdot \gamma_{VFP} \cdot \frac{p_{vVFP}}{p_{vL}}} . \tag{3.25}$$

In Eqs. 3.24 and 3.25 the quantity D_{Ag} denotes the binary diffusion coefficients of different volatile fission products ($A \mathrel{\hat{=}} VFP$) and the solvent L ($L \mathrel{\hat{=}} Na$) in the gas phase (g). The exponent n is the so-called Schmidt number exponent from Eq. 3.10 as well as a correction factor for heat–mass transfer analogy defects c_{1A} and $c_{cond\ A}$ corresponding to Eqs. 3.16 and 3.19.

As a first result, Eq. 3.25 shows that the retention factors RF_{VFP} of the volatile species are practically independent of the pool inventory, depending on transport and fluid properties as well as correction factors only.

3.2 Non–Volatile Species Release

Concerning the release of non–volatile species, based upon optical observations and phenomenological investigations [37–39], the entrainment of liquid droplets with dispersed non–volatile species from the wavy pool surface into a gas flow is identified as the decisive release mechanism for non–volatile species like non–volatile fission products as strontium oxide (SrO) and fuel (uranium dioxide (UO_2)).

The salient features of this pool problem are sketched in Fig. 3. The wave evolution as well as the instabilities in the phase interface boundary layer are originated in the momentum exchange caused by the relative velocity between pool surface and gas flow. Fig. 3a depicts that the convective flow of inert gas with velocity U_∞ causes the development of the pool surface boundary layer thickness δ, together with an increase (evolution) of the wave height.

This wave evolution with droplet generation is depicted in Fig. 3b as a function of the distance x. It is expressed that the wave evolution may be divided into several ranges [40], beginning with no visible disturbances (the velocity profile $u(x, z)$ is plotted at this location) at small distances x, first ripples followed by a non–linear wave growth, wave breaking and droplet generation with increasing distances [41–44]. Furthermore, it is obvious that the initiation of entrainment by wave breaking requires a special kind of waves, namely the so-called roll waves [40, 45]. To form this kind of waves, a minimum distance x, or a minimum gas velocity is needed, respectively.

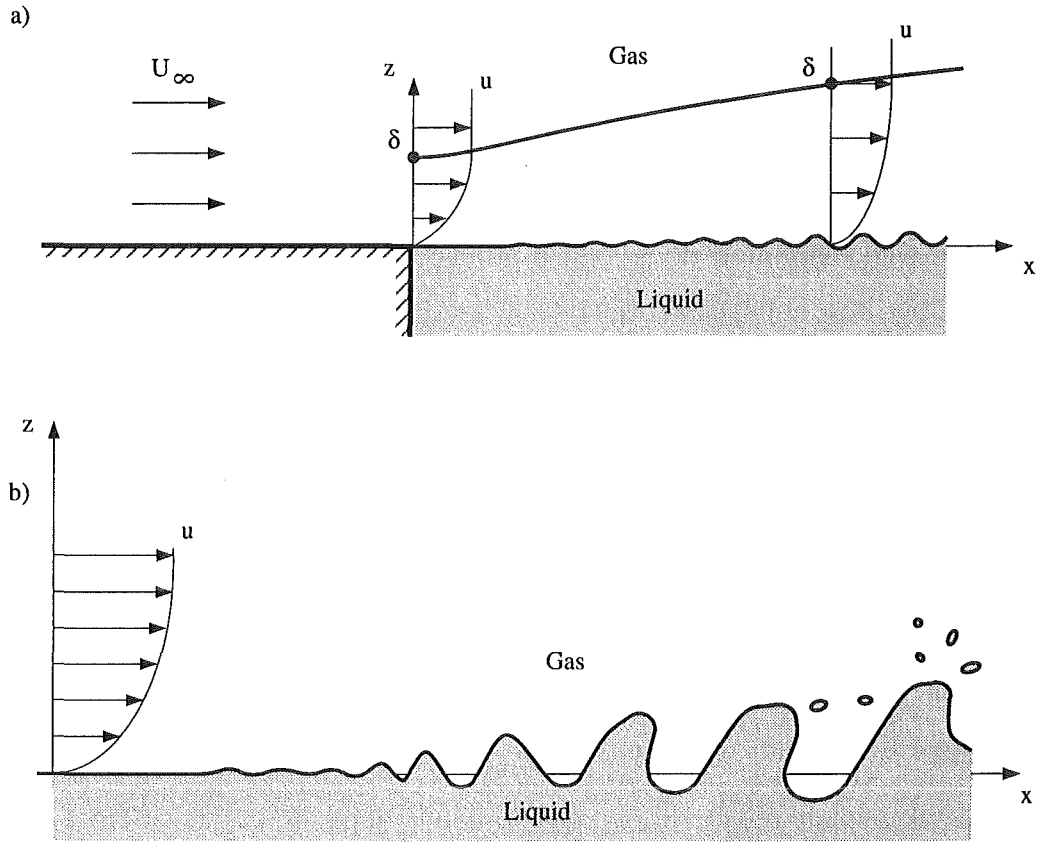

Fig. 3: a.) Sketch of the gas flow parallel to the wavy pool surface, with the free gas velocity U_∞, the velocity profile $u(x, z)$, and the boundary layer thickness δ increasing with the distance x.
b.) Sketch of the wave evolution with droplet generation as a function of distance x and gas convection plotted by the velocity profile $u(x, z)$, with no visible disturbances at small distances and first ripples followed by non–linear wave growth, wave breaking and droplet generation with increasing distance.

The initiation of entrainment is assumed, when a critical value of the gas velocity U_∞ will be reached [46–49]. This means, that the convection conditions — the gas velocity U_∞ is coupled to the friction velocity u_*, see Eq. 3.31 — will have a valuable influence on the beginning of entrainment. A criterion is expressed by the Wave Reynolds number [50, 51], defined as:

$$Re_h = \frac{u_* \cdot h}{\nu_g} \quad , \tag{3.26}$$

with the kinematic velocity ν_g, the effective wave height h, and the friction velocity u_*, the latter coupled with the gas density ρ_g and the shear stresses τ at the phase interface by:

$$u_* = \sqrt{\frac{\tau}{\rho_g}} \quad . \tag{3.27}$$

The influence of the surface tension may be neglected in case of wave lengths in the order of $25\ mm$ and greater, see [40, 45, 52], which is assumed in this model.

The criterion for incipient liquid entrainment results from several water-air experiments as [40, 45, 53]:

$$Re_h = 310 \quad . \tag{3.28}$$

Because the fluid properties (density and kinematic viscosity) of the system sodium—inert gas do not strongly deviate from the related properties of an air-water combination, Eq. 3.28 may be used as a lower bound of droplet entrainment as a first guess for a sodium pool also. This criterion may be used until "in-scale"–sodium experiments will lead to better values.

The upper bound of the mechanistic model for entrainment is given in form of the gas velocity U_∞ of $15\ m/s$ [37, 45, 53]. But this velocity does not influence the use of the mechanistic model, because it is too high for natural convection conditions in case of the reactor accident considered.

The Wave Reynolds number (Eq. 3.26) strongly depends on the effective wave height h. Assuming small wave lengths in comparison to the pool depth, the wave height h is calculated by [40, 45]:

$$h = 0.0178 \cdot u_* \cdot \sqrt{\frac{x}{g}} \quad , \tag{3.29}$$

derived from air-water experiments valid within a range of $1m \leq x \leq 50m$. Eq. 3.29 expresses that the wave height is a function of the friction velocity u_*, the distance x, and the gravitational acceleration g.

For sodium pools, Eq. 3.29 is modified taking into account that the temperature dependent sodium kinematic viscosity directly influences the damping of the large surface waves (surface tension neglected) [54]. Since Eq. 3.29 is based on water experiments at constant temperature [40, 45], the kinematic viscosity is hidden in the constant factor. Using the temperature dependent viscosity of sodium, leads to:

$$h = 1.59 \cdot 10^{-8} \left[\frac{m^2}{s}\right] \cdot \frac{u_* \cdot \rho_{Na}}{\eta_{Na}} \cdot \sqrt{\frac{x}{g}} \quad . \tag{3.30}$$

In fact, the postulated influence of the kinematic viscosity requires further experimental work for comparative assessment.

For the calculation of the Wave Reynolds number now the friction velocity u_* must be evaluated. As written above, the convection above the liquid surface has important influence on this value. This convective flow induces a velocity boundary layer (see Fig. 3a) increasing with the pool length x. The velocity profile inside this layer is assumed to have of a logarithmic shape (experimental results, see [42, 55–57]), comparable to a velocity profile at a rigid wall. Hence, the profile may be divided into two vertical zones, beginning with a region near the liquid surface, where the velocity is visually lower than the gas velocity U_∞, and the remaining area, where the profile approaches the gas velocity asymptotically [37, 51, 58].

Consequently, the analysis of the friction velocity is based on investigations of the velocity boundary layer. As a strongly simplified model the phase interface may be identified as a flat plate; the waves as well as a kind of surface roughness [42, 55–57, 59]. These approximations will lead to similarities (analogy model) between a convective flow over a flat, rough plate and the liquid pool surface considered.

As an example, the most simplified model is given by [8]:

$$u_* = K_\tau \cdot U_\infty \quad , \tag{3.31}$$

with the gas velocity U_∞ outside the boundary layer, and the coefficient K_τ varying between 0.2 and 0.5. Two further models, the profile method [40, 50] and an asymptotic approach [50] have been analyzed to decide, whether the friction velocity u_* is located near the upper or the lower bound of the K_τ interval considered. Because of their complex structure, these approaches are not discussed in detail here, but they are implemented in the Code RENONS.MOD1 together with Eq. 3.31 and:

$$K_\tau \approx 0.2 \quad , \tag{3.32}$$

which will be a sufficient first guess resulting from several RENONS calculations. If improved correlations to calculate the friction velocity will be available, e.g. submitted by the corresponding safety code, additional comparative assessments might be performed.

Hence, the entrainment mass flow $\dot{M}_{EL}$ of the solvent (here sodium) is given by an expression:

$$\dot{M}_{EL} = \frac{\pi}{6} d^3 \cdot \rho_l \cdot b \cdot \int_{z=0}^{z=z_d(x,z)} \dot{n}_d(x,z)\, dz \; , \tag{3.33}$$

using the droplet diameter d (assumed to be spherical), the liquid density ρ_l, the pool width b, and the integral over the droplet–layer height $z_d(x,z)$ of the specific droplet flux $\dot{n}_d$ passing through the vertical plane over the pool, depending on the friction velocity, the wave height (see [40]) and the properties of the fluids considered.

In addition to the geometry and fluid properties as well as the wave height h, the mean diameter d of the droplets entrained and the integral over the droplet–layer height $z_d(x,z)$ of the specific droplet flux $\dot{n}_d$ must be evaluated to calculate the entrainment mass flow $\dot{M}_{EL}$ (Eq. 3.33). Experimental observations lead to widespread spectra of diameters for defined gas velocities and

heights above the pool surface; experimental data are available for air-water combinations, only. The experiments show, that in the region of the pool surface, where the air flow can be assumed to be completely turbulent, the droplet spectrum is independent of both the distance x [60], and the height above the pool surface, where it was analyzed [58]. Hence, the droplet spectrum is assumed to be constant in horizontal and vertical direction neglecting gravitational settling, but dependent on the gas velocity [58, 61]. Evaluated from few discrete data available [58], as a first guess:

$$d = 1.64 \cdot 10^{-5}\,[s] \cdot (U_\infty - 1\,[m/s]) \tag{3.34}$$

can be obtained for the mean droplet diameter d. Because of the lack of data for a system sodium–inert gas (argon or nitrogen), additional experiments are necessary to prove this correlation.

Furthermore, experiments [45] indicate that a logarithmic profile of the droplet flux density (droplets per m^2 and s) $\dot{n}_d(x,z)$ is formed at the distance x considered as a function of the droplet–layer height z. This results in [40, 45]:

$$\dot{n}_d = \dot{n}_{d*} \cdot K^{-1} \cdot \ln\left(\frac{z_d}{z}\right) \quad , \tag{3.35}$$

which can be referred to a normalized specific droplet flux $\dot{n}_{d*}$, being evaluated as [40]:

$$\dot{n}_{d*} = 1.3 \cdot 10^4 \cdot \exp\left(1.25 \cdot 10^4 \cdot Re_{z_d}\right) \quad \left[m^2 s\right]^{-1} \quad , \tag{3.36}$$

with the droplet boundary layer height z_d and the von Karman constant K $(= 0.4)$ [40, 62]. In Eq. 3.36 the Droplet-Layer Reynolds number Re_{z_d} is defined as:

$$Re_{z_d} = \frac{u_* \cdot z_d}{\nu_g} \quad , \tag{3.37}$$

being coupled with the Re_h by [40]:

$$Re_{z_d} = 19.4 \cdot Re_h - 6000 \quad , \tag{3.38}$$

within its limitation to:

$$Re_{z_d} < 40000 \quad . \tag{3.39}$$

As the last missing value for the entrainment flux calculation (Eq. 3.33) the height z_d of the droplet boundary layer can be obtained by rearranging Eq. 3.37.

The entrainment mass flux $\dot{M}_{E\,NFP}$ (index: $NFP \mathrel{\hat{=}}$ Non–Volatile Fission Product or Fuel Particles) of the non–volatile radionuclides considered is coupled to the entrainment mass flux $\dot{M}_{EL}$ by the surface concentration (index: S) of the radionuclides:

$$\dot{M}_{E\,NFP} = c_{NFP\,S} \cdot \dot{M}_{E\,L} \quad . \tag{3.40}$$

As a first approximation, the mass concentration $c_{NFP\,S}$ of non–volatile fission products considered is identified as function of the mean diameter d of the particles and the quotient of the masses of the NFP and the sodium in the top layer of the liquid pool.

Retention Factor

The release of the suspended non–volatile fission products and fuel particles is considered analogous to the reflection of volatile fission products by a retention factor. The retention factor RF_{NFP} of a non–volatile species is given by:

$$RF_{NFP} = \frac{\left(\frac{m_{NFP}}{m_L}\right)_{Pool}}{\left(\frac{\dot{M}_{E\,NFP}}{\dot{M}_L}\right)} = \frac{\left(\frac{m_{NFP}}{m_L}\right)_{Pool}}{\frac{\left(\frac{m_{NFP}}{m_L}\right)_S \cdot \dot{M}_{E\,L}}{\left(\dot{M}_{E\,L} + \dot{M}_{V\,L}\right)}} \quad , \tag{3.41}$$

with the pool inventory m_{APool} of the respective species $A \mathrel{\hat{=}} NFP, L$, the entrainment mass flow $\dot{M}_{E\,NFP}$ of the suspended species, being a product of the concentration $(m_{NFP}/m_L)_S$ of this species at the surface and the entrainment mass flow $\dot{M}_{EL}$ of the liquid, and its release mass flow $\dot{M}_L$, which

is the sum of the entrainment mass flow $\dot{M}_{EL}$ and the release mass flow $\dot{M}_{VL}$ by direct vaporization calculated by the REVOLS code.

In comparison to the evaporative release mass flow $\dot{M}_{VL}$ of the volatile liquid (Chapter 3.1) the liquid entrainment mass flow $\dot{M}_{EL}$ (Chapter 3.2) is negligibly small, so that for a simplification of the calculation the release mass flow $\dot{M}_L$ of the liquid in Eq. 3.41 can be equated with the evaporation mass flow $\dot{M}_{VL}$.

Based on this mechanistic model for liquid entrainment calculation of non–volatile species the code module RENONS is developed.

4 Thermodynamic Properties

To evaluate the fission product release from liquid sodium pools into an inert gas atmosphere, the thermodynamic properties of both the gas and the liquid phase are needed. The code REVOLS.MOD1 contains equations for all species with satisfactory agreement within the range from melting to boiling temperature of sodium at ambient pressure $0.1\ MPa$. However, additional correlations for the code version MOD1.1 presented here (see Chapter 5) are evaluated taking into account an extended pressure range, given as:

$$0.1\ MPa \leq p \leq 0.5\ MPa \quad , \tag{4.1}$$

and a higher gas phase temperature:

$$273\ K \leq T_{g\infty} \leq 1500\ K \quad . \tag{4.2}$$

The thermodynamic properties must be calculated within this new set of system boundaries. Resulting from the higher system pressure (Eq. 4.1), higher pressure dependent saturation temperatures $T_{satA}(p)$ of the pool inventory (sodium and volatile fission products) must be calculated, because incipient pool boiling at saturation condition is assumed to be an upper bound of the mechanistic model.

Hence, all temperature dependent property correlations of the liquid pool inventory are described within two ranges. The first one contains the temperature range up to the saturation temperature of the sodium pool at ambient pressure $T_{satNa}(0.1\ MPa) = 1150\ K$, the second one up to the species dependent saturation temperature $T_{satA}(0.5\ MPa)$ ($A \mathrel{\hat{=}} Na,\ VFP$).

For the gas phase properties, the same distinction of the temperature ranges is used, being more simple in the upper bound temperature (Eq. 4.2).

The thermodynamic properties are presented separately, namely for the inert gas phase in the following Chapter 4.1, and for the pool inventory in Chapter 4.2.

4.1 Gas Phase

Two possible types of inert gases, namely nitrogen (N_2) and argon (Ar) are considered by the code package. For both, the following thermodynamic properties of the gas phase (index $g \widehat{=} Ar,\ N_2$) are prepared:

- Density ρ_g,
- specific heat capacity $c_{p\ g}$,
- thermal conductivity λ_g,
- dynamic viscosity η_g and
- kinematic viscosity ν_g being calculated by the dynamic viscosity η_g divided by the density ρ_g.

At the low pressure level ($0.1\ MPa \leq p \leq 0.5\ MPa$) considered, all properties practically do not depend on the system pressure (with the exception of the density calculations). The properties of the gases are given by tables [63–66]. All correlations are evaluated by an empiric regression analysis of these table values. They show satisfactory agreement with the discrete table data. Details are expressed below in order of the property list given above.

Density

For density calculations, the inert gases are treated as perfect gases. For **argon** holds:

$$\rho_{Ar} = 480.491 \cdot \frac{p}{T} \quad , \tag{4.3}$$

and for **nitrogen**:

$$\rho_{N_2} = 337.005 \cdot \frac{p}{T} \quad , \tag{4.4}$$

with the system pressure p in $[bar]$ and the temperature T in $[K]$.

Heat Capacity

The specific heat $c_{p\ Ar}$ of the mono–atomic **argon** does not depend on the temperature, hence follows to be [63]:

$$\frac{c_{p\,Ar}}{[J/kgK]} = 519 \quad . \tag{4.5}$$

The specific heat $c_{p\ N_2}$ of **nitrogen** is given for two temperature ranges, up to the temperature T of $600K$ as [66]

$$\frac{c_{p\,N_2}}{[J/kgK]} = 0.125 \cdot \frac{T}{[K]} + 1003 \quad , \tag{4.6}$$

and at temperatures exceeding $600K$ to $1500K$ by the equation [66]

$$\frac{c_{p\,N_2}}{[J/kgK]} = 1.196 \cdot 10^3 \cdot \left(\frac{T}{1150\,[K]}\right)^{0.1617} \quad . \tag{4.7}$$

Thermal Conductivity

The thermal conductivity for both of argon and nitrogen is calculated within two temperature ranges, too. For **argon** the equation:

$$\frac{\lambda_{Ar}}{[W/mK]} = 33.00 \cdot 10^{-3} \cdot \left(\frac{T}{673[K]}\right)^{0.7063} \quad , \tag{4.8}$$

is derived from single data in [63] up to the temperature margin $T \leq 1150K$. Within the higher temperature range ($1150K < T \leq 1500K$), the REVOLS–Code uses the correlation (data from [64]):

$$\frac{\lambda_{Ar}}{[W/mK]} = 37.33 \cdot 10^{-3} \cdot \left(\frac{T}{800\,[K]}\right)^{0.6973} \quad . \tag{4.9}$$

Similar to argon the **nitrogen** thermal conductivity is evaluated for the range of $T \leq 1150K$ [63] to

$$\frac{\lambda_{N_2}}{[W/mK]} = 47.00 \cdot 10^{-3} \cdot \left(\frac{T}{673\,[K]}\right)^{0.7014} \tag{4.10}$$

and for higher temperatures ($1150K < T \leq 1500K$) [63] to

$$\frac{\lambda_{N_2}}{[W/mK]} = 52.00 \cdot 10^{-3} \cdot \left(\frac{T}{773\,[K]}\right)^{0.6996} . \tag{4.11}$$

Dynamic Viscosity

The dynamic viscosity of argon and nitrogen is calculated as a function of the film temperature (Eq. 3.7) like all gas phase properties considered. For **argon** at lower temperatures $T \leq 1150K$, the following equation is derived from data given by [63]:

$$\frac{\eta_{Ar}}{[kg/ms]} = 41.00 \cdot 10^{-6} \cdot \left(\frac{T}{673\,[K]}\right)^{0.6769} , \tag{4.12}$$

and for higher temperature values $1150K < T \leq 1500K$ [64]:

$$\frac{\eta_{Ar}}{[kg/ms]} = 47.80 \cdot 10^{-6} \cdot \left(\frac{T}{800\,[K]}\right)^{0.7032} . \tag{4.13}$$

The equation for **nitrogen** is given as

$$\frac{\eta_{N_2}}{[kg/ms]} = 31.40 \cdot 10^{-6} \cdot \left(\frac{T}{673\,[K]}\right)^{0.6591} , \tag{4.14}$$

for $T \leq 1150K$ [63] and for $1150K < T \leq 1500K$ [65] to

$$\frac{\eta_{N_2}}{[kg/ms]} = 34.84 \cdot 10^{-6} \cdot \left(\frac{T}{800\,[K]}\right)^{0.6245} . \tag{4.15}$$

Kinematic Viscosity

The kinematic viscosity does not have an "own" correlation for the inert gases considered. They are evaluated using the correspondent values of the density and the dynamic viscosity from the equations given above by

$$\nu_g = \frac{\eta_g}{\rho_g} . \tag{4.16}$$

Coefficient of Binary Diffusion

Additional to the thermodynamic properties, one transport property, the coefficient of binary diffusion D_{Ag} of the evaporated species A in the atmosphere (index: g), has to be calculated considering the dimensionless groups presented in Chapter 3.1.1.

The coefficient of binary diffusion D_{Ag} of the evaporating species diffusing into a gas mixture (g) containing the species A (for the fission products under consideration taken from [67–72]) and an inert gas ($g \mathrel{\hat{=}} Ar$ or N_2) can be calculated using the following expression [67, 73]:

$$D_{Ag} = 0.18583 \cdot 10^{-6} \cdot \frac{\sqrt{T^3 \cdot \left(\frac{1}{\tilde{M}_A} + \frac{1}{\tilde{M}_g}\right)}}{p \cdot \left[\sigma_{Ag}\right]^2 \cdot \Omega_{D\,Ag}} \quad . \tag{4.17}$$

This equation is valid for low densities and requires the perfect gas law approximation. The coefficient of diffusion D_{Ag} depends on the pressure p (in $[atm]$) of the system, and the temperature T (in $[K]$). Furthermore, $\tilde{M}_A$ (in $[g\ moles^{-1}]$) and $\tilde{M}_g$ (in $[g\ moles^{-1}]$) are the molar weights of the species considered, and σ_{Ag} (in [Å]) is the Lennard-Jones parameter, which represents the atomic radius of the two molecules. The dimensionless function $\Omega_{D\,Ag}$ indicates the energy dependence of the effective collision area, resulting from the Lennard-Jones model [74] for deflecting (diffusing) molecules. $\Omega_{D\,Ag}$ is given by discrete values [67, 73] depending on the temperature and a species' dependent constant ε_{Ag}/k resulting from the Lennard-Jones model [74].

4.2 Liquid Phase

The fluid properties of the liquid pool inventory are calculated for two temperature ranges according to Chapter 4. The maximum temperature has been identified as the pressure dependent saturation temperature (incipient boiling), explained below.

Saturation Temperature

The following correlations to calculate the saturation temperature T_{satA} (index sat: Saturation) of species A are implemented in the current REVOLS-Code version. For the solvent **sodium** (Na) holds [75]:

$$\frac{T_{satNa}}{[K]} = -1.2023 \cdot 10^4 \cdot \left[\ln\left(\frac{p}{10\,[bar]}\right) - 8.1185\right]^{-1}, \tag{4.18}$$

with the system pressure p in $[bar]$ (for shallow pools and phase interface treatment identical to the gas phase pressure p_g). For the volatile fission products **cesium** (Cs) and **rubidium** (Rb) the following equations are derived from single measurement data in [76]:

$$\frac{T_{satCs}}{[K]} = 950 \cdot \left(\frac{p}{1.0981\,[bar]}\right)^{0.11718} \tag{4.19}$$

and

$$\frac{T_{satRb}}{[K]} = 1000 \cdot \left(\frac{p}{1.4739\,[bar]}\right)^{0.11698} \tag{4.20}$$

within the validity range of the system pressure:

$$1\ bar \leq p \leq 5\ bar \quad . \tag{4.21}$$

The saturation temperature T_{satNaI} of the remaining fission product sodium iodide (NaI) does not have to be modelled for high pressure conditions, because the only two property correlations needed (vapor pressure and heat of vaporization) are valid up to $1577K$ exceeding the maximum system temperature of $1500K$ given here. Hence, no additional investigation of the sodium iodide fluid property correlations is needed.

For all other species treated, the saturation– and hence incipient boiling temperature is assumed to be an upper bound of the release model (see pp. 25). The extended system temperature range treated leads to values of the species' vapor pressure exceeding the ambient pressure of $0.1\ MPa$. Consequently,

the correlations for the vapor pressure must be extended to consider higher ambient pressures as follows.

Equilibrium Vapor Pressure

In the mechanistic model the vapor (sodium and/or fission products) at the gas side of the phase interface is assumed to be in saturation condition. Hence, the correlations are divided into two ranges of the phase interface temperature T_{Ph}, the first resulting into vapor pressure values below the species' saturation temperature at the ambient pressure level of $0.1\ MPa$, and the second interval in the temperature range between the saturation temperature at ambient pressure and the saturation temperature T_{satA} at the maximum pressure level ($0.5\ MPa$). The following correlations are used to evaluate the vapor pressure within the range considered, i.e. for the **sodium** vapor pressure p_{vNa} in $[bar]$ at temperatures below $1152\ K$ [21]:

$$\log\left(\frac{p_{vNa}}{[bar]}\right) = \left[6.36 - \frac{5567\ [K]}{T} - 0.5 \cdot \log\left(\frac{T}{[K]}\right)\right], \tag{4.22}$$

and for $1152K \leq T \leq T_{satNa}(p)$ [23]:

$$\frac{p_{vNa}}{[bar]} = 10 \cdot \exp\left[11.2916 - \frac{12532.694\,[K]}{T} - 0.3869 \cdot \ln\left(\frac{T}{[K]}\right)\right]. \tag{4.23}$$

Corresponding to sodium, the two temperature ranges for the vapor pressure p_{vCs} of **cesium** are given as [21]:

$$\log\left(\frac{p_{vCs}}{[bar]}\right) = 3.9429 - \frac{3760\ [K]}{T} \tag{4.24}$$

for $302K \leq T \leq 955K$ and for higher temperatures $955K \leq T \leq T_{satCs}(p)$ by the equation [23]:

$$\frac{p_{vCs}}{[bar]} = 10 \cdot \exp\left[11.0122 - \frac{9011.334\,[K]}{T} - 0.5448 \cdot \ln\left(\frac{T}{[K]}\right)\right]. \tag{4.25}$$

The thermochemical and physical behavior of cesium and rubidium differs only slightly, therefore, the vapor pressure correlations of **rubidium** (Rb) appear to be quite similar to these of Cs:

$$\log\left(\frac{p_{vRb}}{[bar]}\right) = 4.1169 - \frac{3975\ [K]}{T}\,, \tag{4.26}$$

for the range between $312K \leq T \leq 967K$ [21] and

$$\frac{p_{vRb}}{[bar]} = 10 \cdot \exp\left[9.6922 - \frac{9266.648\,[K]}{T} - 0.3388 \cdot \ln\left(\frac{T}{[K]}\right)\right], \tag{4.27}$$

for $967K \leq T \leq T_{satRb}(p)$ [23].

The Eqs. 4.23, 4.25, and 4.27 given above for the corresponding higher temperature intervals are valid indeed within the following temperature ranges [23]:

$$\begin{aligned} Na: &\quad 864\ K \leq T \leq 2361\ K \quad , \\ Cs: &\quad 728\ K \leq T \leq 2045\ K \quad , \\ Rb: &\quad 707\ K \leq T \leq 2073\ K \quad . \end{aligned} \tag{4.28}$$

Therefore they also may be used for partial vapor pressure calculations for fission products in the atmosphere, where higher temperatures than in the liquid pool (e.g. $T_{Ph} < T_{g\infty} = 1500\ K$) are allowed.

The vapor pressure p_{vNaJ} of **sodium iodide** is also given for two ranges, namely for $298K \leq T \leq 933K$ [25]:

$$\log\left(\frac{p_{vNaJ}}{[bar]}\right) = \left[7.557 + \frac{10924\ [K]}{T}\right], \tag{4.29}$$

and for $933K \leq T \leq T_{satNaJ}(p)$ [21]:

$$\log\left(\frac{p_{vNaJ}}{[bar]}\right) = \left[18.0849 - \frac{10740\ [K]}{T} - 3.52 \cdot \log\left(\frac{T}{[K]}\right)\right], \tag{4.30}$$

The validity range of Eq. 4.30 extends to $1577\ K$, it covers the highest possible system temperature assumed to be $1500\ K$.

Additionally to the vapor pressure of the pool inventory, the heat of vaporization is calculated by the REVOLS-Code also, as described as follows.

Heat of Vaporization

For calculation of the condensation within the thermal boundary layer (see Eq. 3.20) the heat of vaporization Δh_{VA} of the fission products and the solvent (Na) are needed. Beginning with the solvent sodium, the heat of vaporization correlations for the pool inventory are explained below.

For **sodium**, it is assumed that the liquid only exists in the mono-atomic state, but in the course of the vaporization the sodium forms molecules [77–80]. The sodium vapor in the inert gas phase is considered to be essentially a mixture of 1–, 2– and 4–atomic molecules [77]. Hence, the heat of vaporization is the sum of the vaporization energies for the single sodium steam mixture components:

$$\Delta h_{VNa} = \frac{X_1 \cdot \Delta h_{V1} + 2 \cdot X_2 \cdot \Delta h_{V2} + 4 \cdot X_4 \cdot \Delta h_{V4}}{X_1 + 2 \cdot X_2 + 4 \cdot X_4} \quad , \tag{4.31}$$

with the heat of vaporization Δh_{Vi} of the components i (i indicates 1–, 2– and 4–atomic molecules) and their molar quantities X_i in the gas phase.

The heat of vaporization Δh_{V1} for mono-atomic sodium at temperature T is given as [77, 80]:

$$\begin{aligned} \frac{\Delta h_{V1}}{[J/kg]} = & 4.73121 \cdot 10^6 - 725.441 \cdot \frac{T}{[K]} + 0.416721 \cdot \frac{T^2}{[K^2]} \\ & - 1.54272 \cdot 10^{-4} \cdot \frac{T^3}{[K^3]} \quad . \end{aligned} \tag{4.32}$$

If poly-atomic sodium is assumed to exist in the vapor phase, the heat of vaporization (Eq. 4.32) must be reduced by their enthalpy of formation Δh_{Fi} (index F: Formation; $i \widehat{=} 2, 4$). That leads to the expression:

$$\Delta h_{Vi} = (\Delta h_{V1} - \Delta h_{Fi}) \, , \tag{4.33}$$

with

$$\frac{\Delta h_{F2}}{[J/kg]} = 1.66663 \cdot 10^6 \tag{4.34}$$

and

$$\frac{\Delta h_{F4}}{[J/kg]} = 1.88835 \cdot 10^6 \quad . \tag{4.35}$$

The mole fraction X_i of sodium molecules is given by the general expression [81]:

$$X_1 + X_2 + X_4 = 1 \quad . \tag{4.36}$$

But the molar amount of the 2– and 4–atomic sodium molecules depends on the temperature so that the mole fractions X_i in Eq. 4.36 are not constant. However, it is assumed that the atomic and the molecular sodium is always in equilibrium, represented by the equilibrium constant k_i ($i \widehat{=} 2, 4$) for each type of molecule. Derived from experimental data, the equilibrium constants k_2 and k_4 are given as:

$$\frac{k_2}{[1/bar]} = \frac{1}{1.01325} \cdot \exp\left(-A_2 + \frac{B_2[K]}{T}\right) \quad , \tag{4.37}$$

and

$$\frac{k_4}{[1/bar^3]} = \frac{1}{1.04028} \cdot \exp\left(-A_4 + \frac{B_4[K]}{T}\right) \quad . \tag{4.38}$$

with the constants in Eq. 4.37 and 4.38 [77]:

$$\begin{aligned} A_2 &= 9.95845; \quad B_2 = 9215.72 \quad , \\ A_4 &= 24.59115; \quad B_4 = 20883.17 \quad . \end{aligned} \tag{4.39}$$

Using following expressions the equilibrium constants are coupled with the mole fractions X_i:

$$\frac{k_2}{[1/bar]} = \frac{X_2}{1.01325 \cdot X_1^2 \cdot p_{vNa}} \quad , \tag{4.40}$$

and

$$\frac{k_4}{[1/bar^3]} = \frac{X_4}{1.04028 \cdot X_1^4 \cdot p_{vNa}^3} \quad . \tag{4.41}$$

Substituting Eqs. 4.40 and 4.41 in Eq. 4.36 results in:

$$1.04028 \cdot p_{vNa}^3 \, k_4 \, X_1^4 + 1.01325 \cdot p_{vNa} \, k_2 \, X_1^2 + X_1 - 1 = 0 \quad . \tag{4.42}$$

This equation can be solved by an iteration method by use of Eqs. 4.37 and 4.38. The correlations for the sodium heat of vaporization may be used up to temperatures of $1686K$ [82], which exceeds the sodium saturation temperature at the maximum pressure level considered ($0.5 \; MPa$) (see also Eq. 4.18).

The heat of vaporization Δh_{VCs} of the fission product **cesium** is given as a function of the temperature T according to [83]:

$$\frac{\Delta h_{VCs}}{[J/kg]} = 606125.42 - 95.4553 \cdot \frac{T}{[K]} \tag{4.43}$$

and for **rubidium** by [84]:

$$\frac{\Delta h_{VRb}}{[J/kg]} = 1021349.76 - 141.0785 \cdot \frac{T}{[K]} \, . \tag{4.44}$$

Both correlations are presented in [83] and [84] without validity range.

The heat of vaporization Δh_{VNaJ} for **sodium iodide** is given by [19]:

$$\frac{\Delta h_{VNaJ}}{[J/kg]} = 1905588.67 - 621.1909 \cdot \frac{T}{[K]} \, . \tag{4.45}$$

The validity range of Eq. 4.45 is limited to:

$$800 \; K \leq T \leq 1260 \; K \quad . \tag{4.46}$$

The correlations above are evaluated by an empiric regression analysis of discrete table data and show satisfactory agreement within the temperature range considered.

Additional Sodium Properties

As given in Chapter 3.1.1, additional fluid properties are needed to evaluate the dimensionless groups of heat and mass transfer. Like for the inert gases, the following required fluid properties of liquid sodium:

- Density ρ_{Na},
- specific heat capacity c_{pNa},
- thermal conductivity λ_{Na},
- dynamic viscosity η_{Na} and
- kinematic viscosity ν_{Na} of sodium consisting of the dynamic viscosity η_{Na} divided by the density ρ_{Na}

are given as follows within the validity range of the temperature T [85]:

$$373.15\ K \leq T \leq 1643.15\ K \quad . \tag{4.47}$$

Density (according to [86]):

$$\begin{aligned} \frac{\rho_{Na}}{[kg/m^3]} &= 1011.6 \ - \ 0.2205 \cdot \frac{T}{[K]} \\ &\quad - 1.9224 \cdot 10^{-5} \frac{T^2}{[K^2]} + 5.6377 \cdot 10^{-9} \frac{T^3}{[K^3]} \quad . \end{aligned} \tag{4.48}$$

Specific heat capacity (according to [85]):

$$\frac{c_{p\,Na}}{[J/kgK]} = 1.6301 \cdot 10^3 - 0.83344 \cdot \frac{T}{[K]} + 4.6281 \cdot 10^{-4} \cdot \frac{T^2}{[K^2]} \quad . \tag{4.49}$$

Thermal conductivity (according to [85]):

$$\frac{\lambda_{Na}}{[W/mK]} = 109.69 - 6.4494 \cdot 10^{-2} \cdot \frac{T}{[K]} + 1.1727 \cdot 10^{-5} \frac{T^2}{[K^2]} \, . \tag{4.50}$$

Dynamic viscosity (according to [85]):

$$\frac{\eta_{Na}}{[kg/ms]} = \exp\left[-5.732 + \frac{5.087 \cdot 10^2 \ [K]}{T} - 4.925 \cdot 10^{-1} \cdot \ln\left(\frac{T}{[K]}\right)\right] \quad . \tag{4.51}$$

The fluid property correlations given above for both the gas and the liquid phase are implemented in the code package REVOLS/RENONS, to calculate the release mass flux and retention factors of both sodium and fission products. The code structure of REVOLS and RENONS is explained in detail by means of flow charts in the next Chapter 5.

5 Release Code Package Structure

The code package REVOLS/RENONS is based on these mechanistic models for volatile and non–volatile species release from pool surfaces into an inert gas atmosphere under conditions of natural or forced convection, as described in Chapter 3.1 for volatile species release as well as in Chapter 3.2 for non–volatile ones.

Both modules of the code package are developed as stand–alone codes coupled by an interface transferring data.

The computer code module REVOLS calculates the release mass fluxes and the retention factors of the volatile species. Figure 4 demonstrates the structure of the REVOLS code including the interface to the coupled RENONS code module.

REVOLS.MOD1 allows for parameter studies identifying the governing parameters influencing the release rates and retention factors. However, due to the complex algebraic expressions treated in REVOLS.MOD1, a simplified fast running version of the code has been developed. Based on the above mentioned parameter studies, exponential series type mathematical correlations for sodium and fission product release have been developed and implemented into the high speed code REVOLS.MOD2.

In case of conditions of higher system pressures and gas phase temperatures up to $1500K$ the extended version of the mechanistic based code REVOLS.MOD1.1, discussed here, may be used for parameter analyses and calculations of mass fluxes or retention factors.

The code RENONS is based on the mechanistic model for liquid entrainment calculations (see Eqs. 3.33 and 3.41) of suspended non–volatile species and liquid sodium from pool surfaces into an inert gas flow at ambient pressure conditions only. Figure 5 illustrates the RENONS code structure including the data transfer of the sodium release mass flux by direct vaporization computed by the module REVOLS (see Fig. 4).

Hence, using the release code package REVOLS/RENONS, the influence of the system temperatures, the pool inventory and the geometry as well as the decisive influence of the thermal–hydraulic conditions on the release rates of volatile and non–volatile species can be investigated.

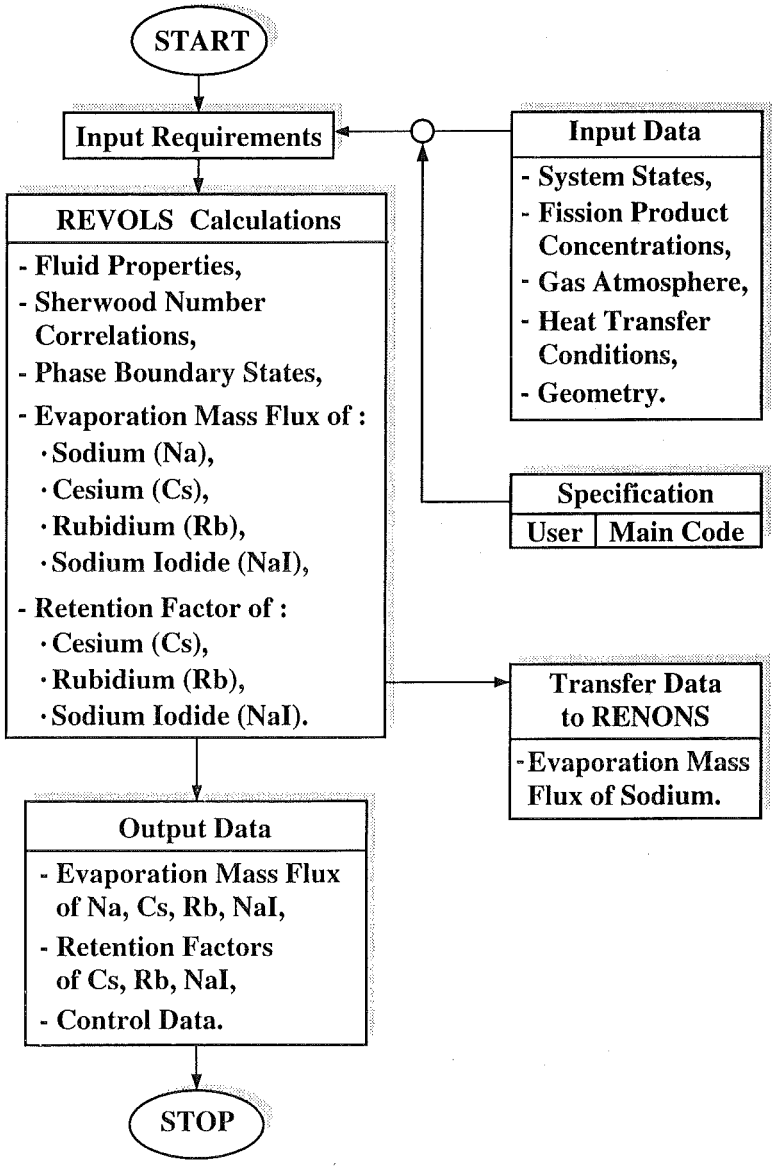

Fig. 4: Flowchart of the computer code REVOLS.MOD1.1 (RElease of VOLatile Species).

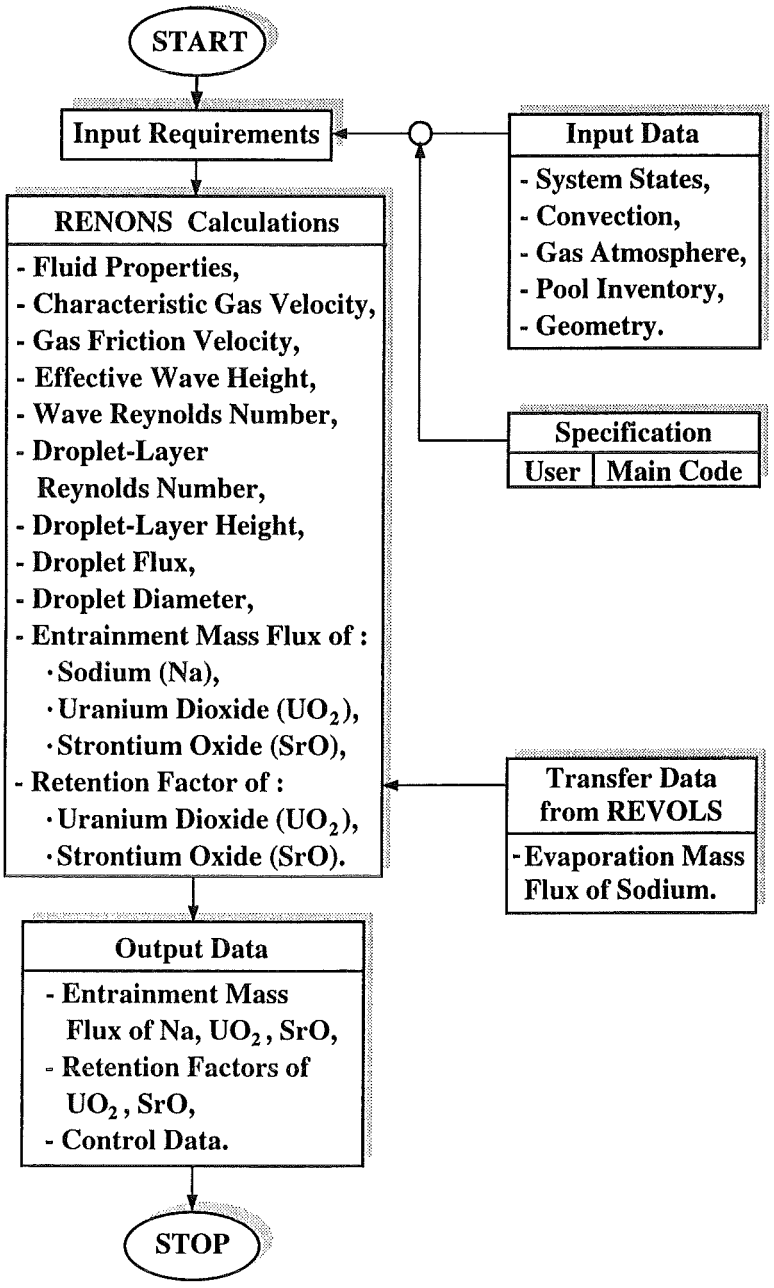

Fig. 5: Flowchart of the computer code RENONS.MOD1 (RElease of NON–volatile Species).

6 Results

The code package has partly been validated by means of a comparison to experimental results, obtained at the Nuclear Research Center Karlsruhe (KfK), Germany. In the following, some selected results are presented as examples. In Fig. 6, a comparison between experimental data [8] of free convection controlled sodium (Na) release (solid dots) from a liquid pool into a $403K$ argon gas atmosphere and the predictions of the mechanistic model (solid line) is presented.

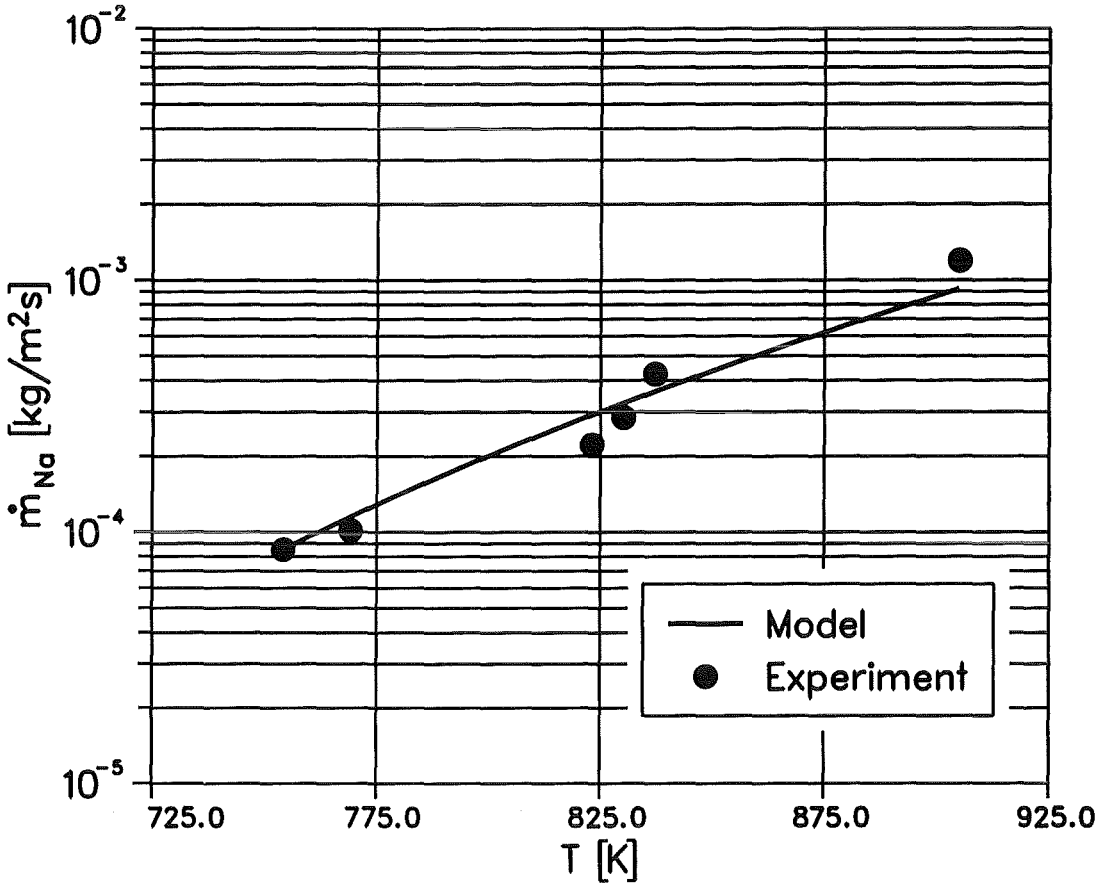

Fig. 6: Free convection controlled release rate $\dot{m}_{Na}$ of sodium from a liquid sodium pool versus the temperature T corresponding to the pool surface temperature T_{Ph}. The solid dots represent the experimental data [8] and the solid line the theoretical results for the release into a $403K$ argon atmosphere.

It can be seen from Fig. 6 that the pool surface temperature T_{Ph} has a decisive influence on the sodium release mass flux $\dot{m}_{Na}$. Theory and experiment are in good agreement.

In Fig. 7, the retention factor RF_{Cs} of cesium (index: Cs) in sodium is plotted versus the temperature of the evaporating surface. The experimental results (solid dots) were taken in an isothermal system with the sodium and cesium release governed by forced convection mass transfer [7].

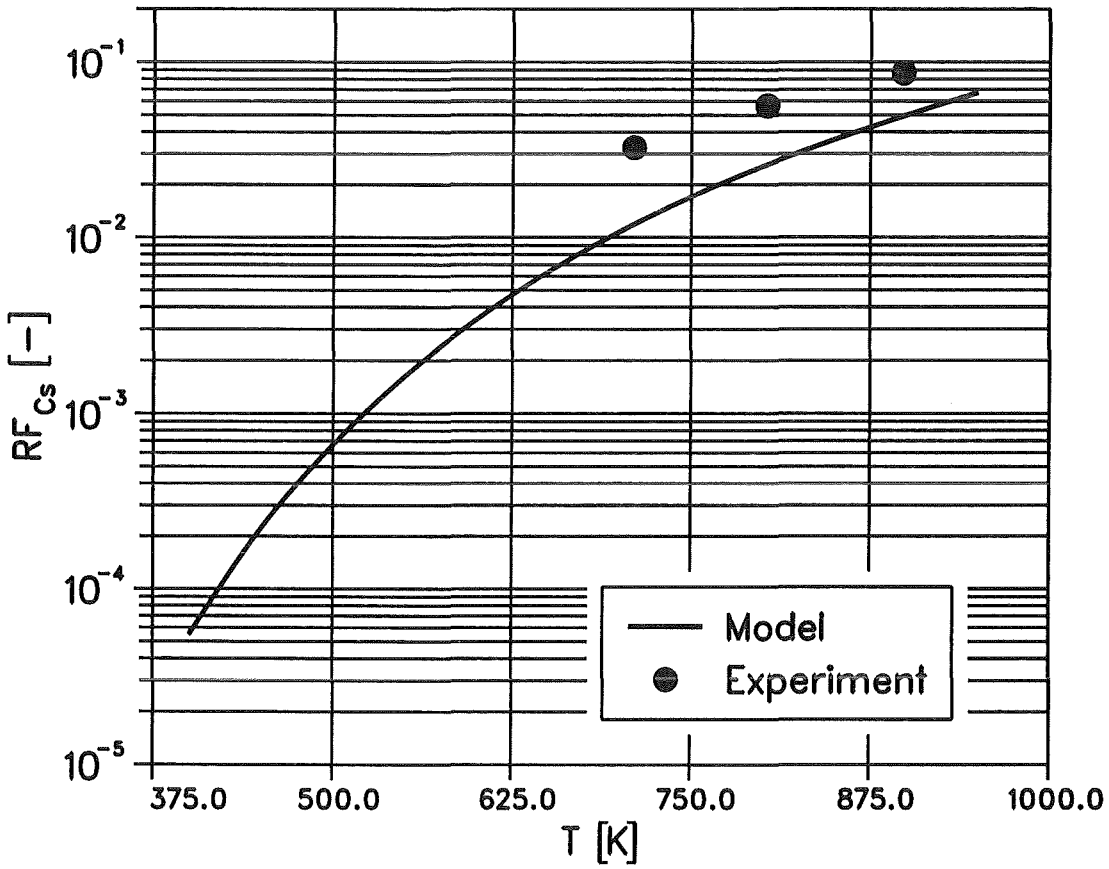

Fig. 7: Retention factor RF_{Cs} of cesium (Cs) in sodium (Na) versus the temperature T corresponding to the pool surface temperature T_{Ph} up to the boiling temperature of cesium ($T_{bCs}(p = 0.1\ MPa) = 955K$). Given are the experimental data [7] for an isothermal system with the mass transport of sodium and cesium governed by forced convection and the corresponding theoretical results.

The solid line represents the theoretical predictions. The retention factor RF_{Cs} of cesium increases with the temperature of the evaporating surface due to an increasing relation between the sodium and the cesium release rate. Satisfactory agreement between theory and experiments is obtained. A reason for the underprediction of the experiments might be due to experimental or theoretical uncertainties, e.g. concerning the temperature history during the experiment or the diffusion coefficient of cesium.

In Fig. 8, the retention factor RF_{NaI} of sodium iodide (index: NaI) in sodium is plotted versus the temperature of the pool surface. Experimental investigations of the sodium iodide release under varying conditions (see [7] and [8], referred to as experiments Nos. 1–3, 5, and 7 under isothermal conditions and Nos. T_1, T_2, and T_4 under conditions of evaporation into a $403K$ gas atmosphere) show a considerable scattering of the retention factor. Due to this situation, the use of a constant retention factor $RF_{NaI} = 3$ has been recommended in [8].

As an example of sodium and volatile fission product release at ambient pressure, Fig. 8 depicts the theoretical results in form of an upper and a lower bound of the range where evaporative release occurs. A meaningful lower bound is an atmospheric temperature of $T_{g\infty} = 300K$ and the upper bound is given by the isothermal case, i.e. the gas temperature reaches the pool temperature ($T_{g\infty} = T_{Ph}$) neglecting external heat sources. The experimental results were expected to lie within this range.

Theoretical investigations now indicate, that two pool temperature ranges may be distinguished on the left and right side of the melting point of pure NaI ($T(p = 0.1\ MPa) \approx 933K$). Whereas in the second temperature range above $933K$ the qualitative behavior of the fission product release could be reproduced satisfactorily by theory, considerable deviations of predicted retention factors compared to those obtained from experiments are observed in the first temperature range below $933K$. These deviations may result from possible different thermodynamic states of NaI, as explained below.

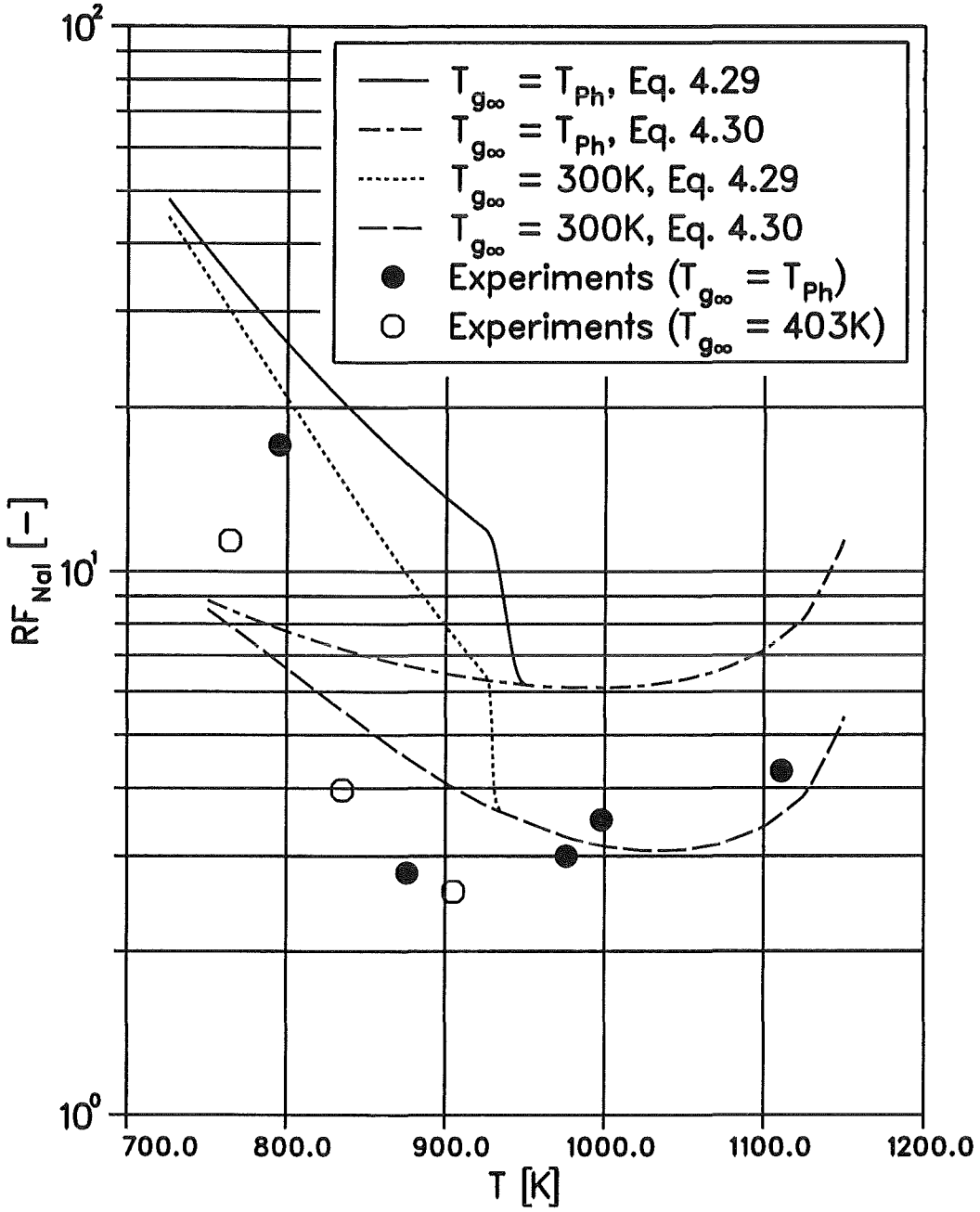

Fig. 8: Retention factor RF_{NaI} of sodium iodide NaI in sodium (Na) versus the temperature T corresponding to the liquid surface temperature T_{Ph}. The theoretical results distinguished by use of different vapor pressure correlations (Eqs. 4.29 and 4.30) in comparison with experimental results [7, 8] mark the possible evaporation temperature range, the upper bound given by the isothermal case ($T_{g\infty} = T_{Ph}$, e.g. mass transfer governed by forced convection), the lower one by constant atmospheric temperature of ($T_{g\infty} = 300K$).

Although the solid state is assumed to exist below $933K$, liquid NaI cannot generally be ruled out, since the pool inventory reflects a binary mixture of practically infinite dilution of NaI in the sodium pool (see Chapter 3.1). Analyzing the corresponding equilibrium phase diagram given in [19], pp. 1738, two partial pressure correlations — either reflecting the solid (Eq. 4.29, [25]) or the liquid (Eq. 4.30, [21]) sodium iodide state — have to be taken into account in case of very small NaI concentrations. Thus, Fig. 8 shows two possible retention factor predictions for the pool temperature range below $933K$, one (the upper) reflecting solid NaI and the other (the lower) reflecting liquid NaI behavior (derived from an extrapolation of Eq. 4.30). The ramp of the respective upper curve at the melting temperature of NaI is caused by a discontinuity at the contact point between the liquid and solid NaI vapor pressure correlations (solidification leads to a transition from Eq. 4.30 to Eq. 4.29). Thus, further investigations especially concerning the partial pressure data and activity coefficient correlations entering the mechanistic model are necessary. Furthermore as can be seen from Fig. 8, the approach based on liquid NaI-data (applying Eq. 4.30 to an extended but uncertain validity range) shows even better agreement between theory and experiments. Nevertheless, due to the lack of more detailed data regarding the mixture sodium-sodium iodide (e.g. phase diagrams for a very small NaI concentration), both correlations seem to be justifiable as a first guess for pool temperatures lower than $933K$.

On the other hand, NaI release below the melting point may as well be governed by mechanisms other than evaporation, like mechanical entrainment. Hence, additional experimental investigations in this range seem to be necessary. In the range above the melting point of sodium iodide with the release rate obviously governed by evaporation of liquid sodium iodide, the agreement is good.

As an example for non–volatile species release, calculated by the RENONS module, the strontium oxide retention factor RF_{SrO} is plotted versus the temperature T in Fig. 9. The theoretical predictions (solid line) are presented for a release, controlled by natural convection from a $10m$ in diameter pool, with a surface concentration of the $1\mu m$ strontium oxide particles of 10% of the average pool concentration into a $403K$ argon atmosphere.

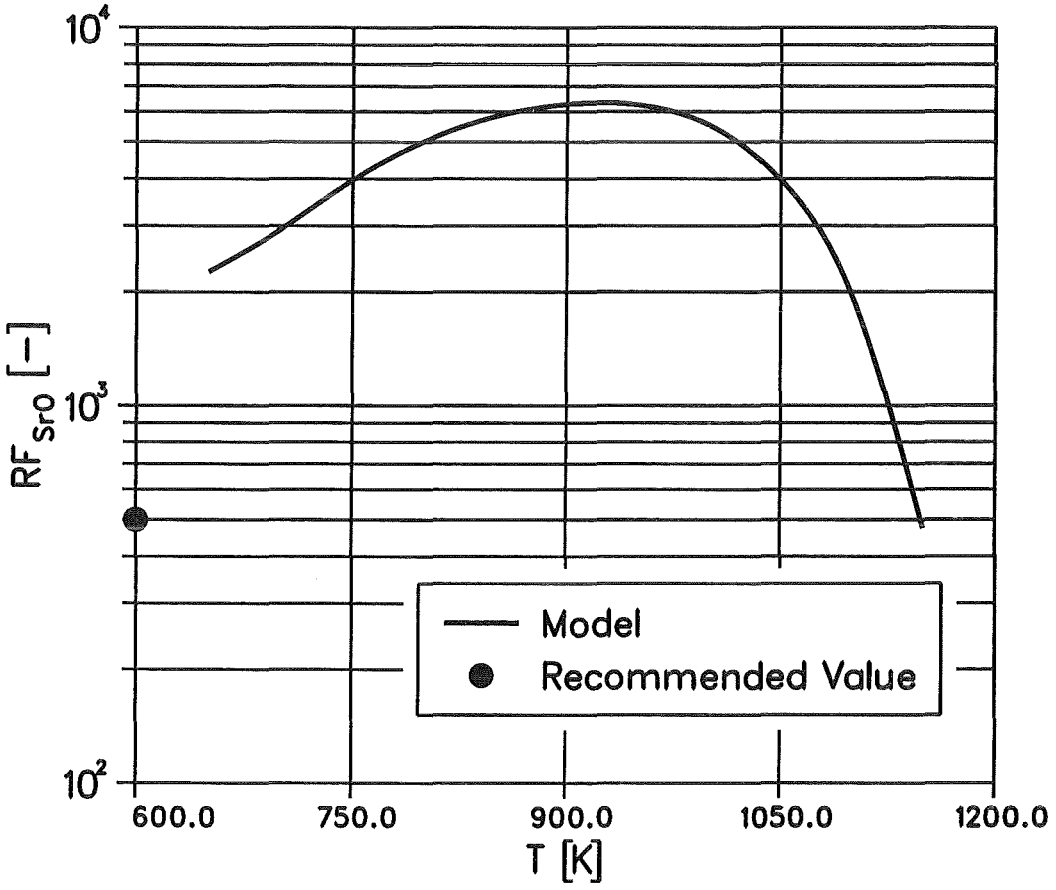

Fig. 9: Retention factor RF_{SrO} of strontium oxide in sodium versus the temperature T corresponding to the liquid pool surface temperature T_{Ph} up to the boiling temperature of sodium ($T_{bNa}(p = 0.1\ MPa) = 1152K$). Given are first theoretical results for a natural convection controlled release into a $403K$ argon atmosphere. The dot at the ordinate marks the recommended value resulting from a conservative estimation of various experimental data [7, 8].

In summarizing various experimental information [7, 8] on SrO release, a conservatively estimated value of the SrO retention factor RF_{SrO} of $5 \cdot 10^{-2}$ (marked by a dot at the ordinate of Fig. 9) was recommended. Fig. 9 shows a decisive influence of the pool surface temperature T on the SrO retention factor RF_{SrO}. An increasing surface temperature causes an increase of the temperature difference between pool surface and gas bulk, which enhances the convection in the gas phase. Up to $950K$, the SrO retention factor increases, caused by a steeper increase of the sodium release rate by direct evaporation based on a steep increase of the vapor pressure, than the SrO entrainment rate. Above $950K$ it decreases however, because the SrO entrainment rate increases steeper with temperature than the sodium evaporation rate, reaching the recommended value based on experimental data near the sodium boiling temperature ($T_{bNa}(p = 0.1\ MPa) = 1152K$).

7 Conclusion

For the improvement of radioactive source term calculations, the code package REVOLS/RENONS has been developed for predicting the release of volatile and non–volatile radionuclides from liquid surfaces into an inert gas atmosphere. Based on mechanistic models, the code package enables release rate calculations under varying system conditions.

Hereby, the module REVOLS evaluates the release of volatile fission products based on a theoretical mechanistic model. The code version REVOLS.MOD1, based on a theoretical mechanistic model, which enables parameter analysis and code improvement, calculates the release in terms of mass fluxes and retention factors of the liquid (sodium) and the volatile species (cesium, rubidium, and sodium iodide) into an inert gas atmosphere consisting of argon or nitrogen. Because of the complex algebraic structure, a fast running code version (REVOLS.MOD2) has been developed. Since new system boundary conditions (higher system pressures and temperatures) appeared, the code version REVOLS.MOD1.1 has been derived from the mechanistic code version MOD1.

The higher temperatures considered result in a different treatment of heat and respective mass transfer situation. The code version REVOLS.MOD1.1 enables handling of "cooler pools/warmer inert gas atmosphere" and vice versa as well as user–defined heat and mass transfer situations (e.g. forced convection). Additionally, the model comprehends presence of sodium in the inert gas atmosphere.

The higher system pressure mostly influences the fluid– and transport properties. Based on the property correlations in the version MOD1, they are extended to a maximum possible system temperature of $1500\ K$ and a pressure range from ambient pressure to $0.5\ MPa$.

A satisfactory agreement between theoretically and experimentally obtained data could be achieved [2, 7, 8].

Hence, the influence of the evaporating surface temperature, the temperature of the atmosphere, the thermal–hydraulic conditions etc. on the release rates can now be investigated theoretically within the ranges given above in good approximation. In addition, upscaling of laboratory data to realistic scenarios becomes possible due to the dimensionless treatment of the governing heat and mass transfer mechanisms as long as thermal–hydraulic similarity exits.

The release of non–volatile fission products and fuel particles like the fission product strontium oxide and the fuel (uranium dioxide) is governed by wave instabilities at the liquid surface. The code RENONS.MOD1 calculates this entrainment release from the pool surface by a parallel gas flow as a function of friction velocity, wave height and fluid properties. The release mechanisms are based upon optic observations of a (sea)water/air interphase and phenomenological investigations. But the lack of sodium data for important values, like diameter of droplets entrained or the effective wave height, lead to a limited application range of the RENONS code, e.g. a restriction to ambient pressure conditions.

Summarizing, the code REVOLS.MOD1.1, which is based on a highly mechanistic model, enables release flux calculations of volatile fission products from a liquid pool into an inert gas atmosphere under variable conditions and user specifications. For both, the release mass flux of the solvent as well as the retention factors of the fission products, satisfactory agreement of the theoretical results with experimental data could be obtained. However, the code RENONS is limited within strict margins, resulting from experimental data restrictions; additional "in–scale" sodium experiments are required for better comparative assessments.

References

[1] U. Brockmeier, M. K. Koch, H. Unger. *A Mechanistic Model for the Prediction of Sodium Release from a Liquid Pool into an Inert Gas Atmosphere*. 1990, pp. 307–318. Proc. of the 1990 International Fast Reactor Safety Meeting, Snowbird, Utah, USA, Vol. 1.

[2] U. Brockmeier, M. K. Koch, W. Schütz, H. Unger. *REVOLS – A Mechanistic Code for the Prediction of Volatile Fission Product Release from Surfaces*. 1991, pp.191 – 195. Proc. of the 1st JSME/ASME Joint International Conference on Nuclear Engineering (ICONE-1), Vol. 2, Tokyo, Japan.

[3] M. K. Koch, U. Brockmeier, W. Schütz, H. Unger. *A Code for the Prediction of Sodium and Volatile Fission Product Release from a Liquid Pool into an Inert Gas Atmosphere*. Journal of Aerosol Science, Special Issue: Proceedings of the 1991 European Aerosol Conference, Karlsruhe, Vol. 22, Suppl. 1, 1991, pp. S709 – S712.

[4] M. K. Koch, U. Brockmeier, W. Schütz, H. Unger. *The Code RENONS for the Prediction of Nonvolatile Species Release from Liquid Surfaces into a Gas*. Journal of Aerosol Science, Special Issue: Proceedings of the 1992 European Aerosol Conference, Oxford, Vol. 23, Suppl. 1, 1992, pp. S835 – S838.

[5] M. K. Koch, J. Starflinger, U. Brockmeier, H. Unger, W. Schütz. *The Release Code Package REVOLS/RENONS for Fission Product Retention Factor Calculation*. 1993, pp. 457-462. Proc. of the 2nd ASME/JSME International Conference on Nuclear Engineering (ICONE-2), Vol. 1, San Francisco, USA.

[6] K. K. Murata. *Recent Developments in the CONTAIN-LMR Code*. In: *Proc. of the 1990 International Fast Reactor Safety Meeting*. Snowbird, Utah, USA, American Nuclear Society, 1990, pp. 261-277.

[7] W. Schütz. UO_2- *und Spaltproduktfreisetzung aus Natriumlachen.* Technischer Fachbericht KfK - 3010, Kernforschungszentrum Karlsruhe, 1980.

[8] H. Sauter, W. Schütz. *Aerosol- und Aktivitätsfreisetzung aus kontaminierten Natriumlachen in eine Inertgasatmosphäre.* Technischer Fachbericht KfK - 3504, Kernforschungszentrum Karlsruhe, 1983.

[9] K. K. Murata, D. E. Carroll, K. E. Washington, F. Gelbard, G. D. Valdez, D. C. Williams, K. D. Bergeron. *User's Manual for CONTAIN 1.1: A Computer Code for Severe Nuclear Reactor Accident Containment Analysis.* NUREG/CR-5026, SAND87-2309R4, Sandia National Laboratories, Albuquerque, New Mexico, USA, 1989.

[10] Gesellschaft für Reaktorsicherheit (GRS) mbH, Hrsg. *Risikoorientierte Analyse zum SNR-300.* GRS - 51, Gesellschaft für Reaktorsicherheit (GRS) mbH, Köln, 1982.

[11] W. S. Clough. *The Behaviour of Barium and Strontium Fission Products in Liquid Sodium.* Technical Report AERE-R-6194, Health Physics and Medical Division, U.K.A.E.A. Research Group, Atomic Energy Research Establishment, Harwell, U.K., 1969.

[12] C. G. Allan. *The Solubilities of Sodium Bromide and Sodium Iodide in Sodium.* TRG Report 2458(D), United Kingdom Atomic Energy Authority. The Reactor Group, 1973.

[13] W. Schröter, K.-H. Lautenschläger, H. Bibrack. *Taschenbuch der Chemie.* Verlag Harri Deutsch: Thun und Frankfurt, 1981.

[14] E. Schmidt. *Technische Thermodynamik, Grundlagen und Anwendungen, Bd. 2, Mehrstoffsysteme und chemische Reaktionen.* Berlin, Heidelberg, New York: Springer-Verlag, 1977.

[15] A. W. Castleman Jr., I. N. Tang, R. A. MacKay. *Fission Product Behavior in Sodium Systems.* In: *USAEC Report BNL-10727.* USAEC, 1966, pp. 729-741. Proceedings IAEA Symposium on Alkali Metal Coolants,

Corrosion Studies and System Operating Experience, Wien, 28.11-2.12.1966.

[16] A. W. Castleman, Jr., I. N. Tang. *Thermodynamics of Fission Product-Sodium Solutions.* Technical Report BNL 11611, Brookhaven National Laboratory, 1968.

[17] W. S. Clough. *The Partition of Iodine between Liquid Sodium and the Gas Phase at* 500^0*C.* Technical Report AERE-R-5848, Health Physics and Medical Division, U.K.A.E.A. Research Group, Atomic Energy Research Establishment, Harwell, U.K., 1968.

[18] K. S. Pitzer. *Solubilities and the Nature of Bonding in Fused Alkali Halide-Metal Systems.* Journal of the American Chemical Society, Vol. 84, No. 11, 1962, pp. 2025-2028.

[19] Gmelin. *Handbuch der anorganischen Chemie: Natrium, Systemnummer: 21, mit Erg.Bd. 1-7.* Weinheim/Bergstr., Berlin: Verlag Chemie GmbH, 1928.

[20] I. Wichterle, J. Linek. *Antoine Vapor Pressure Constants of Pure Compounds.* Prag: Academia, 1971.

[21] I. Barin, O. Knacke. *Thermochemical Properties of Inorganic Substances.* Berlin, Heidelberg, New York, Düsseldorf: Springer-Verlag und Verlag Stahleisen mbH, 1973.

[22] N. A. Lange, G. M. Forker. *Handbook of Chemistry.* New York, Toronto, London: McGraw-Hill Book Company, Inc., 1967.

[23] P. Browning, P. E. Potter. *An Assessment of the Experimentally Determined Vapour Pressures of the Liquid Alkali Metals.* In: *Handbook of Thermodynamic and Transport Properties of Alkali Metals.* R. W. Ohse. International Union of Pure and Applied Chemistry, Chemical Data Series No. 30: Blackwell Scientific Publications, 1985, pp. 349-358.

[24] A. N. Nesmeyanov. *Vapour Pressure of the Elements.* London: Infosearch Limited London, 1963.

[25] G. E. Cogin, G. E. Kimball. *The Vapor Pressures of Some Alkali Halides.* The Journal of Chemical Physics, Vol. 16, 1948, pp. 1035-1048.

[26] K. K. Washington, K. K. Murata, R. G. Gido, F. Gelbard, N. A. Russell, S. C. Billups, D. E. Carroll, R. O. Griffith, D. L. Y. Louie. *Reference Manual for the CONTAIN 1.1: Code for Containment Severe Accident Analysis.* NUREG/CR-5715, SAND91-0835, Sandia National Laboratories, Albuquerque, New Mexico, USA, 1991.

[27] K. D. Bergeron, M. J. Clauser, B. D. Harrison, K. K. Murata, P. E. Rexroth, F. J. Schelling, F. W. Sciacca, M. E. Senglaub, P. R. Shire, W. Trebilcock, D. C. Williams. *User's Manual for CONTAIN 1.0: A Computer Code for Severe Nuclear Reactor Accident Containment Analysis.* NUREG/CR-4085, SAND84-1204, Sandia National Laboratories, Albuquerque, New Mexico, USA, 1984.

[28] M. Al-Arabi, M. K. El-Riedy. *Natural Convection Heat Transfer from Isothermal Horizontal Plates of Different Shapes.* International Journal of Heat and Mass Transfer, Vol. 19, 1976, pp. 1399-1404.

[29] W. M. Lewandowski, P. Kubski. *Methodical Investigation of Free Convection from Vertical and Horizontal Plates.* Wärme- und Stoffübertragung, Nr. 17, 1983, S. 147-154.

[30] O. Krischer, K. Kröll. *Die wissenschaftlichen Grundlagen der Trocknungstechnik.* Berlin, Heidelberg: Springer-Verlag, 1963.

[31] H. Brauer, J. Mühle. *Stoffübertragung bei laminarer Grenzschichtströmung an ebenen Platten.* Chemie-Ing.-Techn., Nr. 39, Heft 5/6, 1967, S. 326-334.

[32] T. Kumada, F. Kasahara, R. Ishiguro. *Sodium Evaporation into a Forced Argon Flow, 1. Measurements of Evaporation under Condition of Fog*

Formation. Journal of Nuclear Science and Technology, Vol. 13, No. 2, 1976, pp. 74-80.

[33] D. E. Rosner. *Enhancement of Diffusion-Limited Vaporization Rates by Condensation within the Thermal Boundary Layer.* International Journal of Heat and Mass Transfer, Vol. 10, 1967, pp. 1267-1279.

[34] C. F. Clement, P. Hartwin. *Transport of Sodium through a Cover Gas of a Sodium Cooled Fast Reactor.* In: *International Conference on Liquid Metal Technology in Energy Production.* Champion, Pennsylvania, 1976, pp. 603-607.

[35] A. W. D. Hills, J. Szekely. *A Note on the Enhancement of the Diffusion Limited Vaporization Rates by Condensation within the Thermal Boundary Layer.* International Journal of Heat and Mass Transfer, Shorter Communications, Vol. 12, 1969, pp. 111-114.

[36] M. Epstein, D. E. Rosner. *Enhancement of Diffusion-Limited Vaporization Rates by Condensation within the Thermal Boundary Layer, 2. Comparison of Homogeneous Nucleation Theory with the Critical Supersaturation Model.* International Journal of Heat and Mass Transfer, Vol. 13, 1970, pp. 1393-1414.

[37] J. Wu. *Spray in the Atmospheric Surface Layer: Review and Analysis of Laboratory and Oceanic Results.* Journal of Geophysical Research, Vol. 84, 1979, pp. 1693-1704.

[38] F. Mayinger. *Strömung und Wärmeübergang in Gas-Flüssigkeits-Gemischen.* Wien: Springer-Verlag, 1982.

[39] H. Langner. *Untersuchungen des Entrainment-Verhaltens in stationären und transienten zweiphasigen Ringströmungen.* Dissertation am Institut für Verfahrenstechnik, Technische Universität Hannover, 1978.

[40] Y. L. Sinai. *A Model of Interfacial Stress and Spray Generation by Gas Flowing Over a Deep, Wavy Pool.* Journal of Fluid Mechanics, Vol. 179,

1987, pp. 327-344.

[41] M. Ishii, M. A. Grolmes. *Inception Criteria for Droplet Entrainment in Two-Phase Concurrent Film Flow.* A.I.Ch.E. Journal, Vol. 21, 1975, pp. 308-318.

[42] T. J. Hanratty, J. M. Engen. *Interaction between a Turbulent Air Stream and a Moving Water Surface.* A.I.Ch.E. Journal, Vol. 3, 1957, pp. 299-304.

[43] S. Ostrach, A. Koestel. *Film Instabilities in Two-Phase Flows.* A.I.Ch.E. Journal, Vol. 11, 1965, pp. 294-303.

[44] T. J. Hanratty, D. E. Woodmansee. *Stability of the Interface for a Horizontal Air-Liquid Flow.* Symposium on Two-Phase Flow, Exeter, Paper A1, 1965, pp. A101-A134.

[45] C. S. Wang, R. L. Street. *Measurements of Spray at an Air-Water Interface.* Dynamics of Atmosphere and Oceans, Elsevier Scientific Publishing Company, Amsterdam, Vol. 2, 1978, pp. 141-152.

[46] G. Hetsroni. *Handbook of Multiphase Systems.* Washington, New York, London: Hemisphere Publishing Corporation, McGraw-Hill Book Company, 1982.

[47] D. E. Woodmansee, T. J. Hanratty. *Mechanism for the Removal of Droplets from a Liquid Surface by a Parallel Air Flow.* Chemical Engineering Science, Vol. 24, 1969, pp. 299-307.

[48] G. B. Wallis. *The Onset of Droplet Entrainment in Annular Gas-Liquid Flow.* Technical Report 62 GL 127, General Electric, General Engineering Laboratory, 1962.

[49] E. C. Monahan. *Sea Spray as a Function of Low Elevation Wind Speed.* Journal of Geophysical Research, Vol. 73, 1968, pp. 1127-1137.

[50] H. Schlichting. *Boundary-Layer Theory, 7th ed.* New York: McGraw-Hill Book Company, 1979.

[51] E. Truckenbrodt. *Fluidmechanik, Bd. II.* Berlin: Springer-Verlag, 1980.

[52] H. Jeffreys. *On the Formation of Water Waves by Wind.* Proceedings of the Royal Society of London, Series A, Vol. 107, 1925, pp. 189-206.

[53] J. Wu. *Sea Spray: a Further Look.* Journal of Geophysical Research, Vol. 87, 1982, pp. 8905-8912.

[54] O. M. Phillips. *The Equilibrium Range in the Spectrum of Wind-Generated Waves.* Journal of Fluid Mechanics, Vol. 4, 1958, pp. 426-434.

[55] G. M. Hidy, E. J. Plate. *Wind Action on Water Standing in a Laboratory Channel.* Journal of Fluid Mechanics, Vol. 26, 1966, pp. 651-687.

[56] J. Wu. *Laboratory Studies of Wind-Wave Interactions.* Journal of Fluid Mechanics, Vol. 34, 1968, pp. 91-111.

[57] J. J. van Rossum. *Experimental Investigation of Horizontal Liquid Films.* Chemical Engineering Science, Vol. 11, 1959, pp. 35-52.

[58] J. Wu. *Spray in the Atmospheric Surface Layer: Laboratory Study.* Journal of Geophysical Research, Vol. 78, 1973, pp. 511-519.

[59] J. S. Hay. *Some Observations of Air Flow over the Sea.* Quarterly Journal of the Royal Meteorological Society, Vol. 81, 1955, pp. 307-319.

[60] C. S. Wang, R. L. Street. *Transfers Across an Air-Water Interface at High Wind Speeds: The Effect of Spray.* Journal of Geophysical Research, Vol. 83, 1978, pp. 2959-2969.

[61] R. J. Lai, O. H. Shemdin. *Laboratory Study of the Generation of Spray Over Water.* Journal of Geophysical Research, Vol. 79, 1974, pp. 3055-3063.

[62] R. B. Bird, W. E. Stewart, E. N. Lightfood. *Transport Phenomena.* New York, London, Sidney: John Wiley & Sons, Inc., 1960.

[63] Verein Deutscher Ingenieure, Hrsg. *VDI-Wärmeatlas, Berechnungsblätter für den Wärmeübergang.* Düsseldorf: VDI-Verlag GmbH, 1984.

[64] V. A. Rabinovich, A. A. Vasserman, V. I. Nedostup, L. S. Veksler. *Thermophysical Properties of Neon, Argon, Krypton and Xenon.* Berlin, New York, London: Springer Verlag, 1988.

[65] E. R. G. Eckert, R. M. Drake. *Analysis of Heat and Mass Transfer.* Washington, New York, London: Hemisphere Publishing Corporation, 1987.

[66] V. V. Sychev, A. A. Vasserman, A. D. Kozlov, G. A. Spiridonov, V. A. Tsymarny. *Thermodynamic Properties of Nitrogen.* National Standard Reference, Data Service of the USSR, A Series of Property Tables: Springer Verlag, 1987.

[67] R. C. Reid, J. M. Prausnitz, B. E. Poling. *The Properties of Gases and Liquids.* New York: McGraw-Hill Book Company, 1987.

[68] Th. W. Chapman. *The Viscosity of Liquid Metals.* A.I.Ch.E. Journal, Vol. 12, 1966, pp. 395-400.

[69] C. J. Smithells, E. A. Brandes, ed. *Metals Reference Book.* London and Boston: Butterworths, 1978.

[70] O. J. Foust, ed. *Sodium-NaK Engineering Handbook, Vol. I, Sodium Chemistry and Physical Properties.* New York: Gordon and Breach, Science Publishers, Inc., 1972.

[71] I. N. Tang, A. W. Castleman Jr., H. R. Munkelwitz. *The Transport of Fission-Product Cesium from Sodium.* Advances in Chemical Series, Radionuclides in the Environment, Vol. 93, 1970, pp. 71-82.

[72] A. D. Pasternak, D. R. Olander. *Diffusion in Liquid Metals.* A.I.Ch.E. Journal, Vol. 13, 1967, pp. 1052-1057.

[73] J. O. Hirschfelder, C. F. Curtiss, R. B. Bird. *Molecular Theory of Gases and Liquids.* New York: John Wiley & Sons, Inc., 1964.

[74] J. E. Jones. *On the Determination of Molecular Fields, II. From the Equation of a State Gas.* In: *Proceedings of the Royal Society.* Series A,

Vol. 106, London, 1924, pp. 473-477.

[75] K. K. Murata, D. E. Carroll, K. D. Bergeron, G. D. Valdez. *CONTAIN LMR/1B-Mod.1, A Computer Code for Containment Analysis of Accidents in Liquid-Metal-Cooled Nuclear Reactors.* SAND91-1490, Sandia National Laboratories, Albuquerque, New Mexico, USA, 1991.

[76] K. Hornung. *Adiabatic and Isothermal Compressibility in the Liquid State.* In: *Handbook of Thermodynamic and Transport Properties of Alkali Metals.* R. W. Ohse. International Union of Pure and Applied Chemistry, Chemical Data Series No. 30: Blackwell Scientific Publications, 1985, pp. 487-524.

[77] G. H. Golden, J. V. Tokar. *Thermophysical Properties of Sodium.* Technical Report ANL-7323, Argonne National Laboratory, 1967.

[78] M. Makansi, W. A. Seike, C. F. Bonilla. *Thermodynamic Properties of Sodium.* Journal of Chemical and Engineering Data, Vol. 5, No. 4, 1960, pp. 441-452.

[79] W. H. Evans, R. Jakobson, T. R. Munson, D. D. Wagman. *Thermodynamic Properties of Alkali Metals.* Journal of Research of the National Bureau of Standards, Vol. 55, No. 2, Research Paper 2608, 1955, pp. 83-96.

[80] N. B. Vargaftik, L. D. Voljak. *Thermodynamik Properties of Alkali Metal Vapours at Low Pressures.* In: *Handbook of Thermodynamic and Transport Properties of Alkali Metals.* R. W. Ohse. International Union of Pure and Applied Chemistry, Chemical Data Series No. 30: Blackwell Scientific Publications, 1985, pp. 535–576.

[81] H. D. Baehr. *Thermodynamik.* Berlin, New York, Heidelberg: Springer-Verlag, 1981.

[82] J. P. Stone, C. T. Ewing, J. R. Spann, E. W. Steinkuller, D. D. Williams, R. R. Miller. *High-Temperature Properties of Sodium.* Technical Report NRL Report 6241, U.S. Naval Research Laboratory, Washington, 1965.

[83] Gmelin. *Handbuch der anorganischen Chemie: Caesium, Systemnummer: 25.* Weinheim/Bergstr., Berlin: Verlag Chemie GmbH, 1928.

[84] Gmelin. *Handbuch der anorganischen Chemie: Rubidium, Systemnummer: 24.* Weinheim/Bergstr., Berlin: Verlag Chemie GmbH, 1928.

[85] M. R. Granziera, M. S. Kazimi. *A Two-Dimensional, Two-Fluid Model for Sodium Boiling in LMFBR Fuel Assemblies.* Energy Laboratory Report No. MIT-EL 80-011, Massachusetts Institute of Technology, 1980.

[86] H. Böse. *Nachwärmeabfuhr aus einem Schnellbrüterkern mit kastenlosen Brennelementen.* Dissertation an der Fakultät für Maschinenbau, Ruhr-Universität Bochum, 1990.

Subject Index

S

T

U

V

W